

# Validation and diagnostic study of cloudburst events over the Himalayan region using IMDAA and ERA5

Nitin Lohan, Ashish Routray, Rohan Kumar, Biranchi Kumar Mahala & Sushil Kumar

**To cite this article:** Nitin Lohan, Ashish Routray, Rohan Kumar, Biranchi Kumar Mahala & Sushil Kumar (2025) Validation and diagnostic study of cloudburst events over the Himalayan region using IMDAA and ERA5, *Geomatics, Natural Hazards and Risk*, 16:1, 2446589, DOI: [10.1080/19475705.2024.2446589](https://doi.org/10.1080/19475705.2024.2446589)

**To link to this article:** <https://doi.org/10.1080/19475705.2024.2446589>



© 2025 The Author(s). Published by Informa UK Limited, trading as Taylor & Francis Group.



Published online: 09 Jan 2025.



Submit your article to this journal



Article views: 2073



View related articles



View Crossmark data



Citing articles: 3 View citing articles

## Validation and diagnostic study of cloudburst events over the Himalayan region using IMDAA and ERA5

Nitin Lohan<sup>a</sup>, Ashish Routray<sup>b</sup>, Rohan Kumar<sup>c</sup>, Biranchi Kumar Mahala<sup>d</sup> and Sushil Kumar<sup>a</sup>

<sup>a</sup>Department of Applied Mathematics, School of Vocational Studies and Applied Sciences, Gautam Buddha University, Greater Noida, India; <sup>b</sup>National Centre for Medium Range Weather Forecasting (NCMRWF), MoES, Noida, UP, India; <sup>c</sup>Department of Earth Sciences, Uppsala University, Uppsala, Sweden; <sup>d</sup>School of Applied Sciences (Mathematics), Kalinga Institute of Industrial Technology (KIIT), Deemed to be University, Bhubaneswar, Odisha, India

### ABSTRACT

A cloudburst is characterised by intense localised rainfall over a brief period, often resulting in significant damage, particularly in high-elevation areas like the Himalayan region. Consequently, it is crucial to anticipate these disastrous events to avoid the associated damage. The objective is to compare the performance of two reanalysis datasets i.e. Indian Monsoon Data Assimilation and Analysis (IMDAA) and fifth-generation European Centre for Medium-Range Weather Forecasts (ERA5), to comprehend the atmospheric dynamics associated with the cloudburst events over the Himalayan region. Four cloudburst cases are analysed during the Southwest Monsoon season, affecting areas at elevations between 1600 and 2100 meters. Daily accumulated rainfall from both reanalyses is compared with the Global Precipitation Measurement (GPM). The results indicate that IMDAA outperforms ERA5, with a mean Pearson correlation of 0.56 versus 0.35, though both datasets underestimate rainfall. IMDAA shows a minor underestimation with a mean bias of  $-0.74\text{ mm}$ , while ERA5 underestimates more significantly, with a mean bias of  $-2.52\text{ mm}$ . Additionally, various atmospheric parameters, including vertically integrated moisture transport, relative humidity, wind fields, potential vorticity, outgoing longwave radiation, and various instability indices, are analysed to investigate the mechanisms behind these cloudburst events. Overall, the high-resolution IMDAA reanalysis outperformed the low-resolution ERA5.

### ARTICLE HISTORY

Received 2 May 2024  
Accepted 19 December 2024

### KEYWORDS

Cloudburst; reanalyses datasets; monsoon; Himalayas; instability indices

## 1. Introduction

Cloudburst events are characterised by rapid and intense rainfall exceeding 100 mm/hr over a compact area of about 20–30 square kilometres (Das et al. 2006). These events have been reported frequently worldwide for several years with extreme

**CONTACT** Rohan Kumar  [rohan.kumar@geo.uu.se](mailto:rohan.kumar@geo.uu.se); Ashish Routray  [ashishroutray@ncmrwf.gov.in](mailto:ashishroutray@ncmrwf.gov.in)

© 2025 The Author(s). Published by Informa UK Limited, trading as Taylor & Francis Group.

This is an Open Access article distributed under the terms of the Creative Commons Attribution License (<http://creativecommons.org/licenses/by/4.0/>), which permits unrestricted use, distribution, and reproduction in any medium, provided the original work is properly cited. The terms on which this article has been published allow the posting of the Accepted Manuscript in a repository by the author(s) or with their consent.

precipitation. The extreme rainfall in one-day event has increased significantly in many countries over the past 100 years (Burton et al. 1993). India is one of the world's most cloudburst- and flood-prone nations. In recent decades, several parts of India have experienced frequent cloudbursts, most notably in the Himalayan region (Kumar et al. 2018). Many of these events end with unpredicted heavy downpours. Consequently, the complex topography and unstable slopes are vulnerable to flash floods and landslides after a cloudburst or heavy rainfall event in the Himalayan region (Upadhyaya et al. 2024). The consequences of a cloudburst often lead to significant damage to property, loss of life among humans and animals, and destruction of essential infrastructure.

Moreover, the occurrence of such events in the Himalayan region during the monsoon season is not abnormal. Most cloudburst events occur during the peak of the Indian monsoon in July and August (Bhan et al. 2004). The cloudburst events over the Himalayan region are often associated with westward-moving cyclonic circulation in the middle troposphere (about 500 hPa) over the Tibet-Ladakh region during the peak of the monsoon (Bhan et al. 2015). One of the primary causes of disastrous downpours in the area, such as those observed in Uttarakhand in 2013 and Jammu and Kashmir in 2014, is the interaction of eastward-moving mid-tropospheric westerly trough and the low-level westward-moving monsoonal system (Ray et al. 2015; Sikka et al. 2015).

Several case studies have investigated the atmospheric dynamics behind major cloudburst events, such as the deadly cloudburst in Leh on 6 August 2010, which resulted in 250 deaths and the destruction of over 1700 houses (Ashrit 2010; Kumar et al. 2012; Thayyen et al. 2013). Other events, like the catastrophic cloudburst in Kedarnath, Uttarakhand, on 16–17 June 2013, which claimed over 6500 lives, have been the focus of multiple studies (Mishra and Srinivasan 2013; Asthana and Asthana 2014; Shekhar et al. 2015). In addition, numerous studies have employed numerical weather prediction (NWP) models to simulate and understand cloudburst events better (Devan et al. 2024; Garg et al. 2024).

In recent years, the role of satellite data has increased in monitoring and predicting cloudburst events. Satellite-based nowcasting techniques have been particularly effective in forecasting extreme rainfall events over the Western Himalayan region, improving early warning systems (Shukla et al. 2017). Similarly, Shah et al. (2023) validated satellite-based cloudburst alerts, demonstrating high location precision over Uttarakhand. Additionally, low values of outgoing longwave radiation (OLR) are often observed preceding cloudburst events, signalling enhanced convection and moisture accumulation (Kripalani et al. 1991; Kumar et al. 2022; Sarkar et al. 2024).

Cloudburst events are often discussed in abundant research articles but are not well defined because of the lack of information and understanding of the characteristics of the cloudburst (Dimri et al. 2017). Recently, many studies have highlighted the crucial role of reanalyses products in gaining insights into precipitation patterns, particularly in challenging and varied terrains where direct observational data is limited. These reanalyses products, however, come with certain limitations. These datasets often fail to accurately capture the intensity of precipitation at higher elevations and during extreme weather events (Palazzi et al. 2013; Bannister et al. 2019). This

underestimation is primarily attributed to the coarse resolution of the data and the smoothing effects produced by complex assimilation algorithms that process the information (Hiemstra et al. 2006; Gutmann et al. 2012; Currier et al. 2017). Such issues become significantly pronounced in mountainous regions, where elevation, weather patterns, and topography create unique precipitation dynamics.

Researchers have increasingly embraced dynamic downscaling techniques in response to the limitations of reanalyses datasets. This innovative approach focuses on refining coarse-resolution reanalyses datasets, such as the widely utilised ERA5, by employing regional climate models (RCMs) like the Weather Research and Forecasting Model (WRF) (Maussion et al. 2011; Bannister et al. 2019; Wang et al. 2021). These models work to improve spatial resolution, which in turn enhances the accuracy of precipitation estimates. RCMs effectively simulate atmospheric processes at higher spatial resolutions, enabling them to resolve small-scale climate variations influenced by complex geographical features such as mountains, valleys, and water bodies (Norris et al. 2020; Gumber and Ghosh 2022; Ghosh et al. 2023). This enables researchers to develop a more nuanced understanding of weather patterns and their impacts.

The current study explores the characteristics of various parameters related to cloudburst events by comparing reanalysis datasets of the European Centre for Medium-Range Weather Forecasts (ERA5) and the Indian Monsoon Data Assimilation and Analysis (IMDAA). While regional climate models provide high-resolution insights, this study utilises reanalyses datasets, ERA5 and IMDAA, to assess the dataset offering the most reliable baseline for subsequent dynamical downscaling in regional climate models. Therefore, this study evaluates the performance of ERA5 and IMDAA in reproducing these high-impact events and highlights the strengths and weaknesses of each dataset in representing such extreme weather events in complex terrain through four cloudburst events.

The data and methodology used in the present study are provided in [Section 2](#). The synoptic features for all four cases are discussed in [Section 3](#). The results and discussion from the comparison of reanalysis datasets are lucidly presented in [Sections 4](#) and [5](#) presents the concluding remarks along with future scope.

## **2. Data and methodology**

### **2.1. Study area**

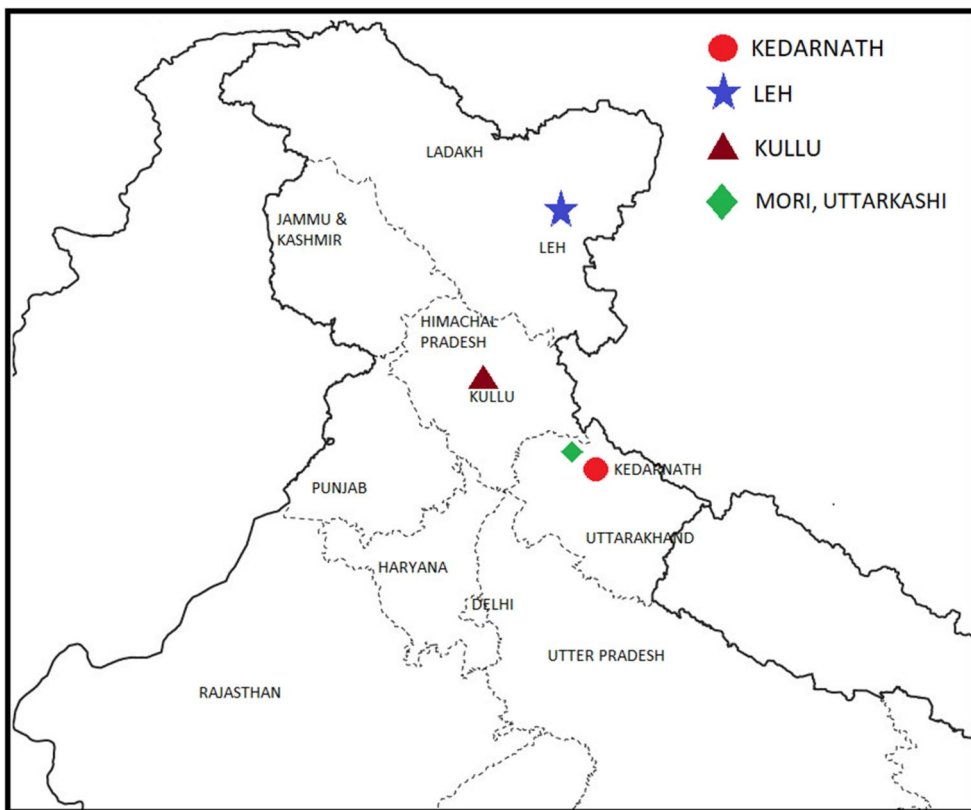
Four cloudburst events were selected for this study, which occurred in the northwest Himalayas. The events' details and associated areas are depicted in [Table 1](#) and [Figure 1](#), respectively.

### **2.2. Datasets**

Four types of datasets, namely experimental datasets of ERA5, IMDAA, satellite data of Integrated Multi-satellite Retrievals for Global Precipitation Measurements (GPM), and observational datasets of IMD for rainfall, are used in the present study. The detail of each dataset is provided from (i) to (iv):

**Table 1.** List of four cloudburst events.

Cloudburst events	Case study	Duration	Location	Damage
16–17 June 2013	A	15–17 June 2013	Kedarnath (30.73°N, 79.07°E)	6600 People, 370 houses (Mishra and Srinivasan 2013)
6 August 2010	B	4–7 August 2010	Leh (34.15°N, 77.58°E)	255 People, 1749 houses (Bhan et al. 2015)
16 July 2003	C	15–17 July 2003	Shilagarh, Kullu (31.5°N, 77° E)	35 People (Das et al. 2006)
18 August 2019	D	17–19 August 2019	Mori, Uttarkashi (31.01°N, 78.05°E)	21 People (Khanduri and Sajwan 2019)

**Figure 1.** Locations impacted by cloudburst for the present study.

- i. The ERA5 dataset, produced by the European Centre for Medium-Range Weather Forecasts (ECMWF), is the fifth-generation global atmospheric reanalysis dataset. ERA5 provides comprehensive climate and weather data using advanced 4D-Var (four-dimensional variational data assimilation) techniques. ERA5 datasets are accessible on standard latitude-longitude grids at  $0.25^\circ \times 0.25^\circ$ , and climate parameters are available on 37 pressure levels. The value of instantaneous variables corresponds to the exact time, and accumulation variables are amassed over an hour before the reported time (Hersbach et al. 2020).

Data is available at <https://cds.climate.copernicus.eu/#!/search?text=ERA5&type=dataset>

- ii. The IMDAA is the result of a joint program of the National Centre for Medium-Range Weather Forecasting (NCMRWF), the Met-Office UK, and the IMD with funding from the National Monsoon Mission project of the Ministry of Earth Sciences, Government of India. Regional analysis over India is carried out using a high resolution of  $0.12^{\circ} \times 0.12^{\circ}$ , with 63 vertical levels reaching a height of about 40km (Rani et al. 2021). Data is available at: <https://rds.ncmrwf.gov.in/datasets> from 1979 onwards.
- iii. Global precipitation measurement (GPM) is a satellite mission launched by the National Aeronautics and Space Administration (NASA) and the Japanese Aerospace Exploration Agency (JAXA) in February 2014 (Huffman et al. 2015). The GPM is a follow-on to the Tropical Rainfall Measuring Mission (TRMM), carrying advanced radar and radiometer systems to observe global precipitation. It provides datasets of daily accumulated high-quality precipitation from all MW sources and daily accumulated precipitation from the microwave-IR estimates since March 2014. Version 5 dataset is available at a spatial resolution of  $0.1^{\circ} \times 0.1^{\circ}$  and a processing level 3 (Huffman et al. 2015). Data is available at: [https://disc.gsfc.nasa.gov/datasets/GPM\\_3IMERGDL\\_06/summary?keywords=%22IMERG%20late%22](https://disc.gsfc.nasa.gov/datasets/GPM_3IMERGDL_06/summary?keywords=%22IMERG%20late%22)
- iv. A new and very high spatial resolution ( $0.25^{\circ} \times 0.25^{\circ}$ ) long period (1901–2019) daily gridded rainfall data over India is prepared by IMD. This data is organised in  $135 \times 129$  grid points. The first data in the record is at ( $66.5^{\circ}\text{E}, 6.5^{\circ}\text{N}$ ); the second is at ( $66.75^{\circ}\text{E}, 6.5^{\circ}\text{N}$ ), and so on. The last data record is ( $100^{\circ}\text{E}, 38.5^{\circ}\text{N}$ ) (Pai et al. 2014).

Data is available at: [https://www.imdpune.gov.in/Clim\\_Pred\\_LRF\\_New/Grided\\_Data\\_Download.html](https://www.imdpune.gov.in/Clim_Pred_LRF_New/Grided_Data_Download.html)

### **2.3. Methodology**

There is no sufficient technique to predict heavy precipitation/cloudbursts in the region with the complex structure of mountains because of the highly nonlinear and complex relationship between meteorological variables (Dimri et al. 2017). Numerical Weather Prediction (NWP) models often fail to capture or predict these extreme events due to less availability of high-resolution data networks over the region with complex orography. The present study compares two reanalysis datasets' performance from four cloudburst cases over the Himalayan region. Vertical integrated moisture flux Q can be expressed as  $Q = \frac{1}{g} \int_0^{p_s} q V dp$  (Ullah and Gao 2012). Where g is the acceleration due to gravity,  $p_s$  is surface pressure, V is wind vector, and q is specific humidity. For vertically integrated moisture transport (VIMT), vertical integration of this equation is carried out from surface pressure in hPa to 300 hPa since specific humidity has a negligible effect above this level and is not a part of the reanalyses (Kalnay et al. 1996).

Also, this study uses the GPM dataset as the truth dataset, known for its reliable precipitation estimates, especially where ground-based data still need improvement.

**Table 2.** Pearson correlation coefficient and MBE for all selected cloudbursts.

Cloudburst Event	Day	Correlation coefficient (ERA5)	Correlation coefficient (IMDAA)	MBE – ERA5 (mm)	MBE – IMDAA (mm)
Cloudburst 'A'	1	0.45	0.61	4.84	6.14
	2	0.43	0.42	-4.54	-2.11
	3	0.53	0.66	-9.70	-3.08
Cloudburst 'B'	1	0.19	0.48	1.53	4.36
	2	0.20	0.59	0.12	1.10
	3	0.58	0.61	-1.71	0.15
Cloudburst 'C'	1	0.22	0.47	-2.5	-0.40
	2	0.45	0.71	1.25	0.63
	3	0.31	0.58	0.9	-0.03
Cloudburst 'D'	1	0.15	0.49	1.36	2.75
	2	0.39	0.57	-15.65	-12.95
	3	0.32	0.51	-6.13	-5.38
Mean		0.35	0.56	-2.52	-0.74

The correlation coefficients and statistical metrics in Table 2 compare ERA5 and IMDAA precipitation data against GPM. IMDAA and GPM datasets were interpolated to match ERA5's spatial resolution, ensuring uniformity and enhancing the accuracy of our evaluations across different spatial scales. This consistent approach is crucial for accurately assessing precipitation patterns and intensities during cloudburst events.

Moreover, the thermodynamic indices are calculated from the following methods:

### 2.3.1. Total Totals Index (TT)

The Total Totals Index combines the Vertical Totals (VT) and Cross Totals (CT), which assess the vertical temperature gradient and the moisture content in the lower atmosphere. This index is convenient for evaluating the strength of the storm but cannot consider the latent instability below 850 hPa (Miller 1975).

$$TT = (T_{850} - T_{500}) + (Td_{850} - T_{500})$$

where  $T_{850}, T_{500}$  are the environment temperature at 850 and 500 hPa, respectively.  $Td_{850}$  is dew point temperature at 850 hPa.

### 2.3.2. Severe Weather Threat Index (SWEAT)

Miller 1975 proposed the SWEAT index for observing severe weather conditions.

$$SWEAT = 12(Td_{850}) + 20(TT - 49) + 2(f_{850}) + f_{500} + 125[(\sin(d_{500} - d_{850})) + 0.2]$$

where  $f_{500}, f_{850}$  are the wind magnitude at 500 and 850 hPa, respectively in knots, and  $d_{850}, d_{500}$  are the wind direction in degrees at 850 and 500 hPa, respectively. This Index includes wind shear, moisture, and instability to identify the potential for severe convective storms. This index is particularly relevant for cloudburst studies, emphasising wind dynamics, which can significantly influence moisture transport and convergence during these events. Its application to cloudburst cases in the Himalayan region highlights the importance of dynamic forcing in triggering intense precipitation (Khanal et al. 2023).

### 2.3.3. Index K (KI)

The K index evaluates atmospheric instability by considering temperature and dewpoint gradients in the lower and mid-troposphere. A higher K index value indicates a greater likelihood of convective activity. For the Himalayan region, elevated K index values have been associated with intense convection during cloudburst events, as demonstrated in recent studies on monsoon-related extreme precipitation (Khanal et al. 2023). This index helps in measuring the potential of thunderstorm clouds (George 1960).

$$KI = (T_{850} - T_{500} - T_{700}) + (Td_{850} + Td_{700})$$

### 2.3.4. Lifted Index (LI)

This index measures the thermal instability of the atmosphere at the mid-troposphere by considering the temperature of the air parcel and environmental temperature (Tyagi et al. 2011).

$$LI = T_{500} - T_{parcel}$$

where  $T_{parcel}$  is the temperature of the air parcel when it is lifted with the dew point temperature, pressure, and average temperature from 500 m ( $T_{500}$ ) above the surface.

The critical values for all these indices are provided in Table 3.

### 2.3.5. Statistical tools

By comparing ERA5 and IMDAA to GPM data, ‘relative strengths and weaknesses can be determined in representing extreme precipitation events over complex terrain with these datasets. This evaluation is particularly critical for understanding how well these datasets capture cloudburst events’ localised and intense nature. Among the various methods available for such analysis, this study employed the Pearson Correlation Coefficient and Mean Bias Error (MBE) to assess their performance. The Pearson correlation coefficient and MBE were calculated between the IMDAA and ERA5 rainfall datasets against GPM data.

- i. Pearson’s correlation: The Pearson correlation coefficient measures the strength and direction of the linear relationship between two variables. For two variables,  $X$  (predicted) and  $Y$  (observed), it is calculated as:

$$r = \frac{\sum (x_i - \bar{x})(y_i - \bar{y})}{\sqrt{\sum (x_i - \bar{x})^2 \sum (y_i - \bar{y})^2}}$$

**Table 3.** Critical levels of stability indices.

Sl.No	Stability index	Description	Critical level
1.	Total totals (TT)	$(T_{850} - T_{500}) + (Td_{850} - T_{500})$	$\geq 48.1$ (Kunz 2007)
2.	SWEAT index	$12(Td_{850}) + 20(TT - 49) + 2(f_{850}) + f_{500} + 125[(\sin(d_{500} - d_{850}) + 0.2]$	$\geq 300$ (Schultz 1989)
3.	K index (°C)	$(T_{850} - T_{500} - T_{700}) + (Td_{850} + Td_{700})$	$\geq 33$ (Litta and Mohanty 2008)
4.	Lifted index	$T_{500} - T_{parcel}$	$\leq -3$ (Litta and Mohanty 2008)

Where  $x_i$  and  $y_i$  are the individual data points,  $\bar{x}$  and  $\bar{y}$  are the means of the predicted and observed values, respectively. A positive value indicates a direct correlation, while a negative value indicates an inverse relationship (Kagone et al. 2023).

- ii. MBE: The MBE indicates the average difference between the predicted and observed values, indicating whether the reanalysis data overestimates or underestimates the observed rainfall. The formula is:

$$MBE = \frac{1}{n} \sum_{i=1}^n (X_i - Y_i)$$

Where  $n$  is the total number of data points,  $X_i$  is the predicted rainfall and  $Y_i$  is the observed rainfall. A positive bias indicates that the reanalysis data overestimates rainfall compared to observations, while a negative bias indicates that the reanalysis data underestimates rainfall (Kagone et al. 2023).

### 3. Associated synoptic conditions with cloudburst

#### 3.1. June 2013

The mean surface pressure chart of IMD, valid 00UTC of 15 and 16 June 2013 (Figure 2(a,b)), clearly shows that the low-pressure monsoon system moved north-westward during that period and merged with the monsoon trough. This led to heavy rainfall in mid-June 2013 in Uttarakhand, which caused a disastrous flood and landslides in that region. This was the worst natural adversity in the Himalayan region and led to the death of more than 6600 people. The water level in the rivers, namely

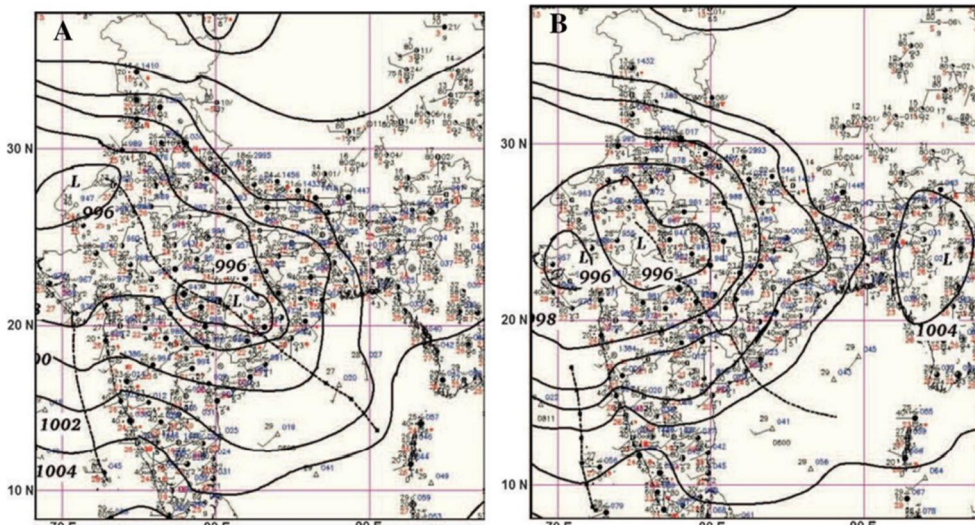


**Figure 2.** IMD mean surface pressure chart valid for 00UTC of 15th and 16th June 2013 respectively (Pratap et al. 2020).

Mandakini and Alknanda, was very high due to continuous rainfall in that region. This event is named Cloudburst 'A' in this study.

### 3.2. August 2010

Heavy rainfall occurred over the Leh region during 5–6 August 2010, which caused a flash flood in the Leh region at Indus Valley in northwest India. This flash flood led to the death of more than 250 people and heavy loss of property. The storm was generated by daytime heating over the Tibetan Plateau grouped into a mesoscale convective system (MCS), then 500 hPa winds, directed over the ridge of Indus Valley, and then the storm draws upon low-level moisture arriving from the Arabian Sea and Bay of Bengal (BoB). This moisture and MCSs merge while passing over Leh and thus produces heavy rainfall. For these MCSs, strong diurnal forcing was responsible, which is quite evident from the images of Meteosat-7 (Figure 3). This cloudburst is named 'Cloudburst B' in the present study.

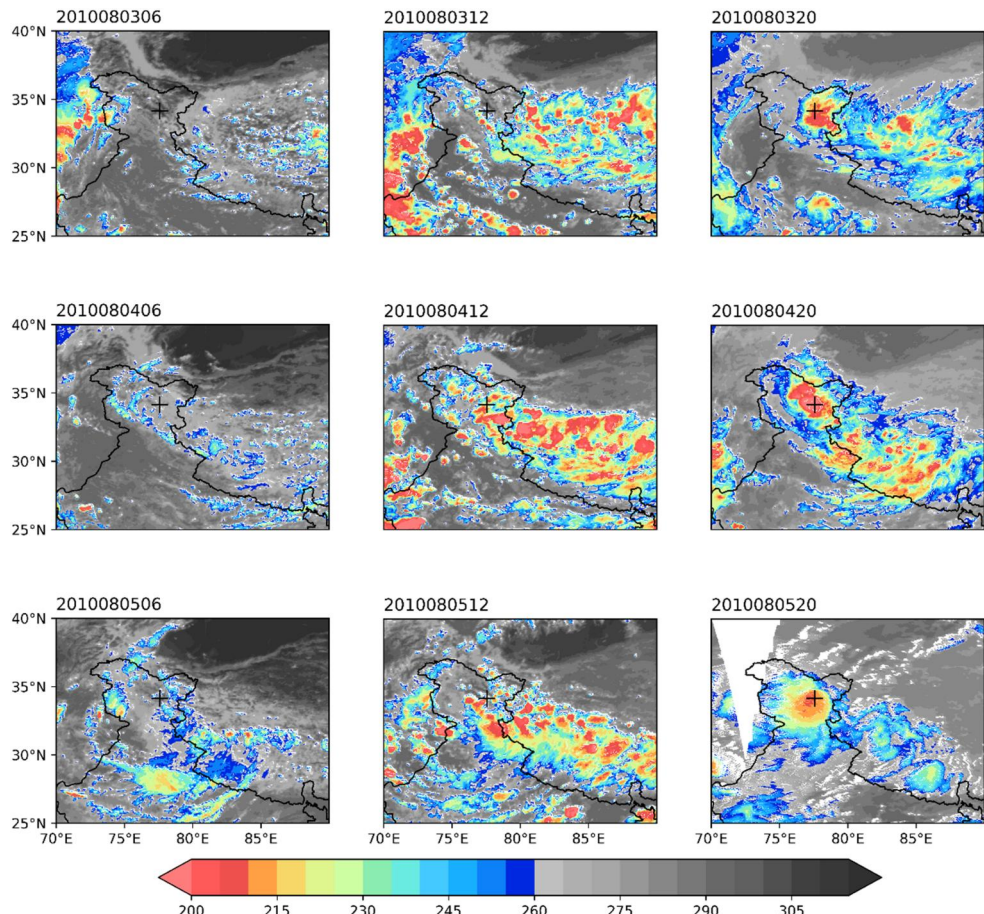


**Figure 3.** Meteosat-7, infrared brightness temperature (K) shows storm systems' evolution resulting from the Leh flood. The date and time are on each plot. A '+' symbol on each plot indicates the location of Cloudburst.

### 3.3. July 2003

On 16 July 2003, heavy rainfall occurred in the Kullu district of Himachal Pradesh. The event affected Shilagarh village (Das et al. 2006). The cloudburst occurred between 3 h and 4 h IST, destroying roads and properties and causing loss of lives (Das et al. 2006). A low-pressure area near Kullu on 15 July 2003 played a pivotal role in creating favourable conditions for this event. The 500-hPa wind pattern indicated vital moisture transport from the Bay of Bengal (BoB), merging with the moist westerly flow from the Pakistan region. This confluence of moisture-laden air streams and local orographic lifting likely contributed to the intense convective activity associated with the cloudburst. Such synoptic-scale interactions highlight the influence of large-scale circulation and mesoscale dynamics in triggering these localised extreme events. This event is named ‘Cloudburst C’.

### 3.4. August 2019

The cloudburst event ‘D’ occurred in Mori, Uttarkashi, on 17–18 August 2019. Thermal infrared satellite imagery from INSAT-3D captured the evolution of the cloud system over the region (Figure 4). The formation of convective clouds began around 17 UTC on 17 August 2019, as they migrated from the plains of Rajasthan, Delhi, and Haryana towards the Uttarkashi region. By 22 UTC on 17 August, cloud density had intensified significantly, persisting until approximately 02 UTC on 18 August 2019, resulting in a heavy downpour. The event was marked by a significant influx of moisture at lower levels, primarily influenced by a well-defined monsoonal

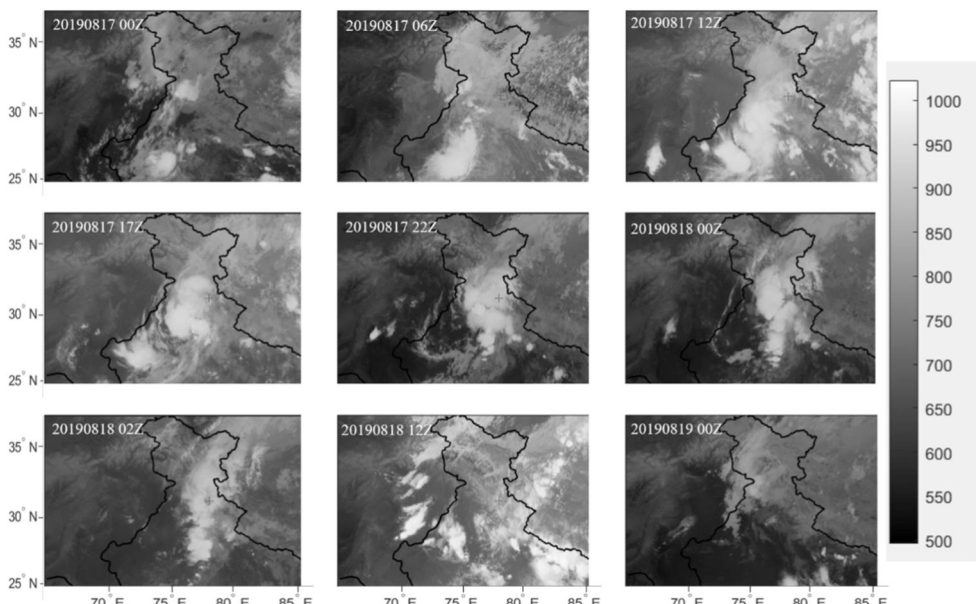


**Figure 4.** The sequence of thermal infrared (TIR grey count) satellite images from INSAT-3D shows clouds' formation over Mori, Uttarkashi region. The ‘+’ symbol indicates the location on each image.

low over the plains. This situation, combined with the orographic effects of the Himalayan terrain, intensified convective instability, ultimately leading to a localised cloudburst.

## 4. Result and discussion

### 4.1. Precipitation analysis

The spatial distribution of accumulated daily rainfall (mm/day) for cloudburst ‘A’ from ERA5, IMDAA, GPM, and IMD datasets is shown in Figure 5(a–l). The cloudburst ‘A’

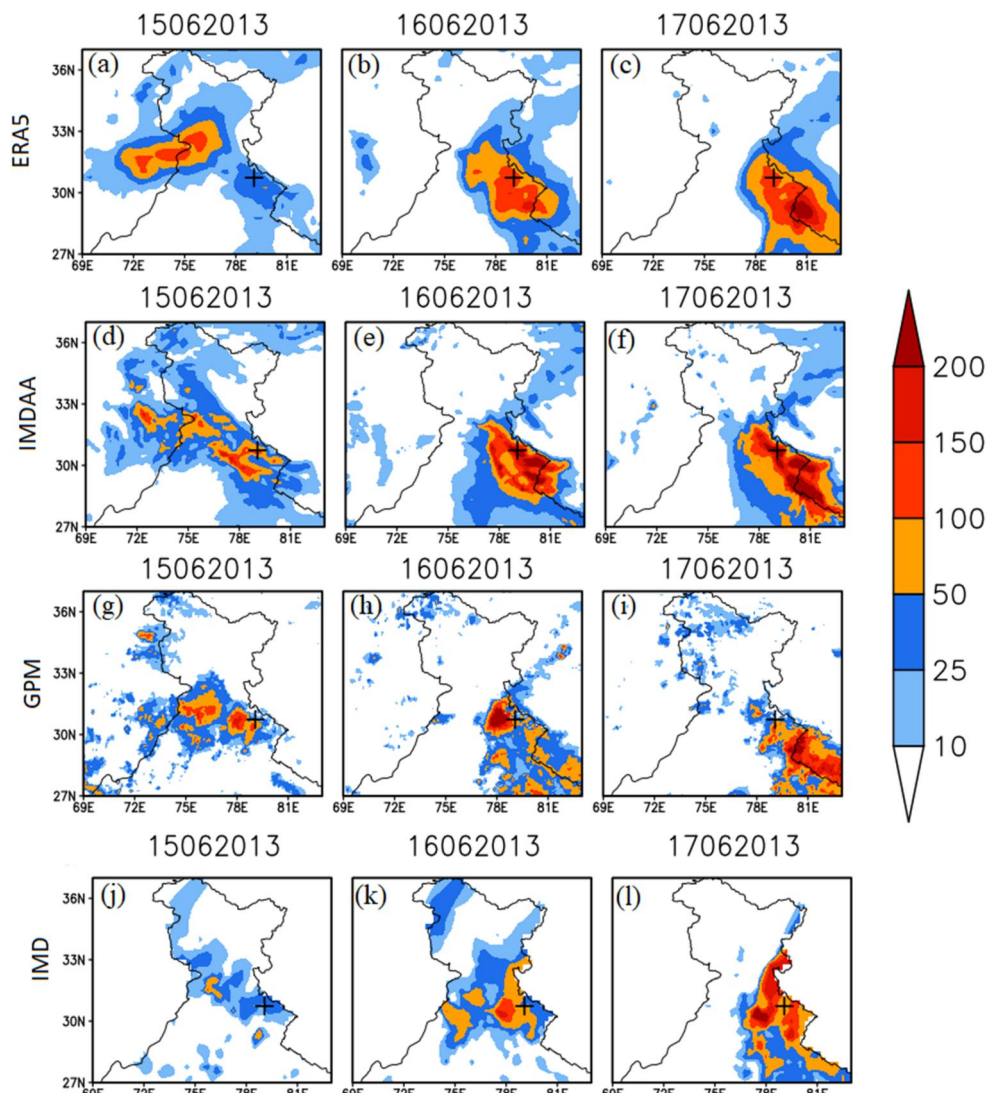


**Figure 5.** Daily accumulated rainfall (shaded, mm/day) for cloudburst ‘A’, (a–c) is from ERA5 datasets, (d–f) is from IMDAA datasets, (g–i) is from GPM datasets, (j–l) is from IMD datasets. The date is mentioned on top of every plot. Location is marked with the symbol ‘+’.

occurs late on the night of 16 June 2013 and early on the morning of 17 June 2013, as per IST. ERA5 captured approximately 140 mm of rainfall on 16–17 June (Figure 5(a–c)). However, IMDAA captured higher accumulated precipitation, with about 220 and 230 mm of accumulated precipitation on 16–17 June, respectively, as seen in Figure 5(d–f). Both datasets capture the maximum rainfall location close to the cloudburst site. The time series of 3-hourly accumulated rainfall over the study region of cloudburst ‘A’ for datasets ERA5, IMDAA, and GPM is shown in Figure 6(a).

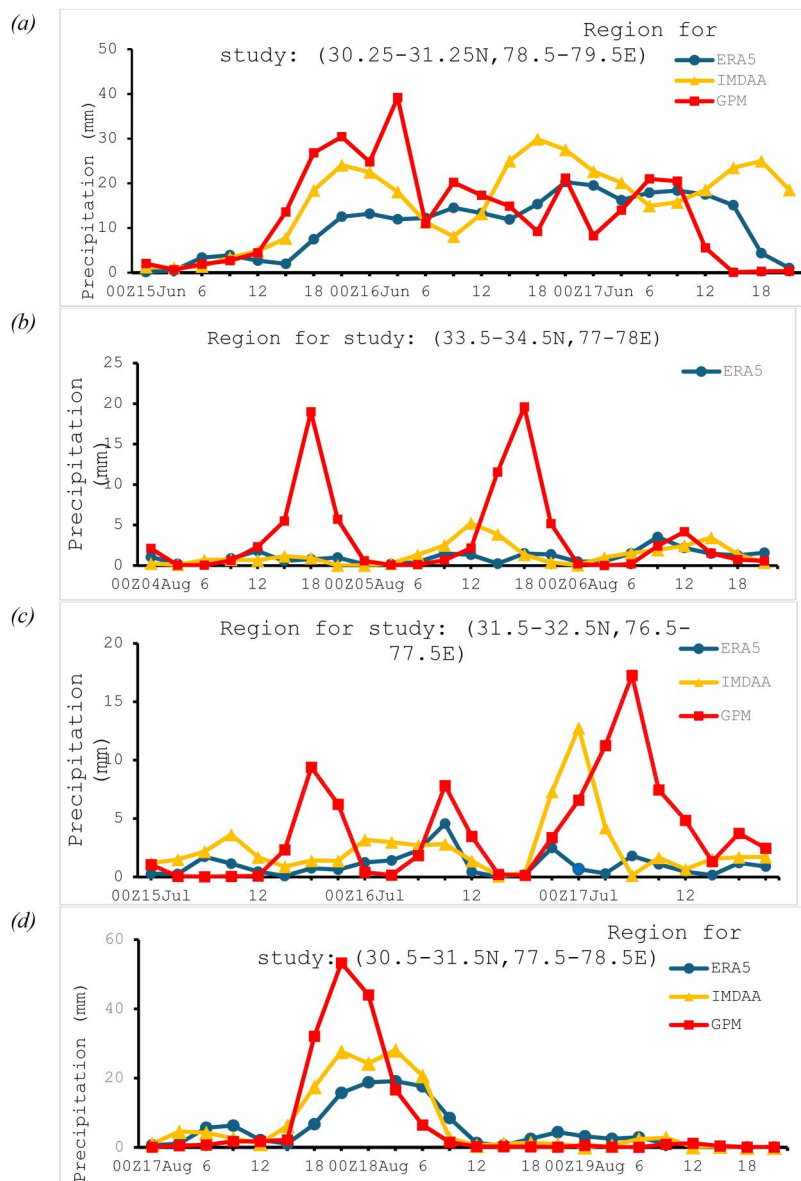


**Figure 6.** Comparison of 3 hourly average precipitation (mm) for (a) cloudburst ‘A’, (b) cloudburst ‘B’, (c) cloudburst ‘C’, (d) cloudburst ‘D’ from ERA5, IMDAA and GPM datasets.

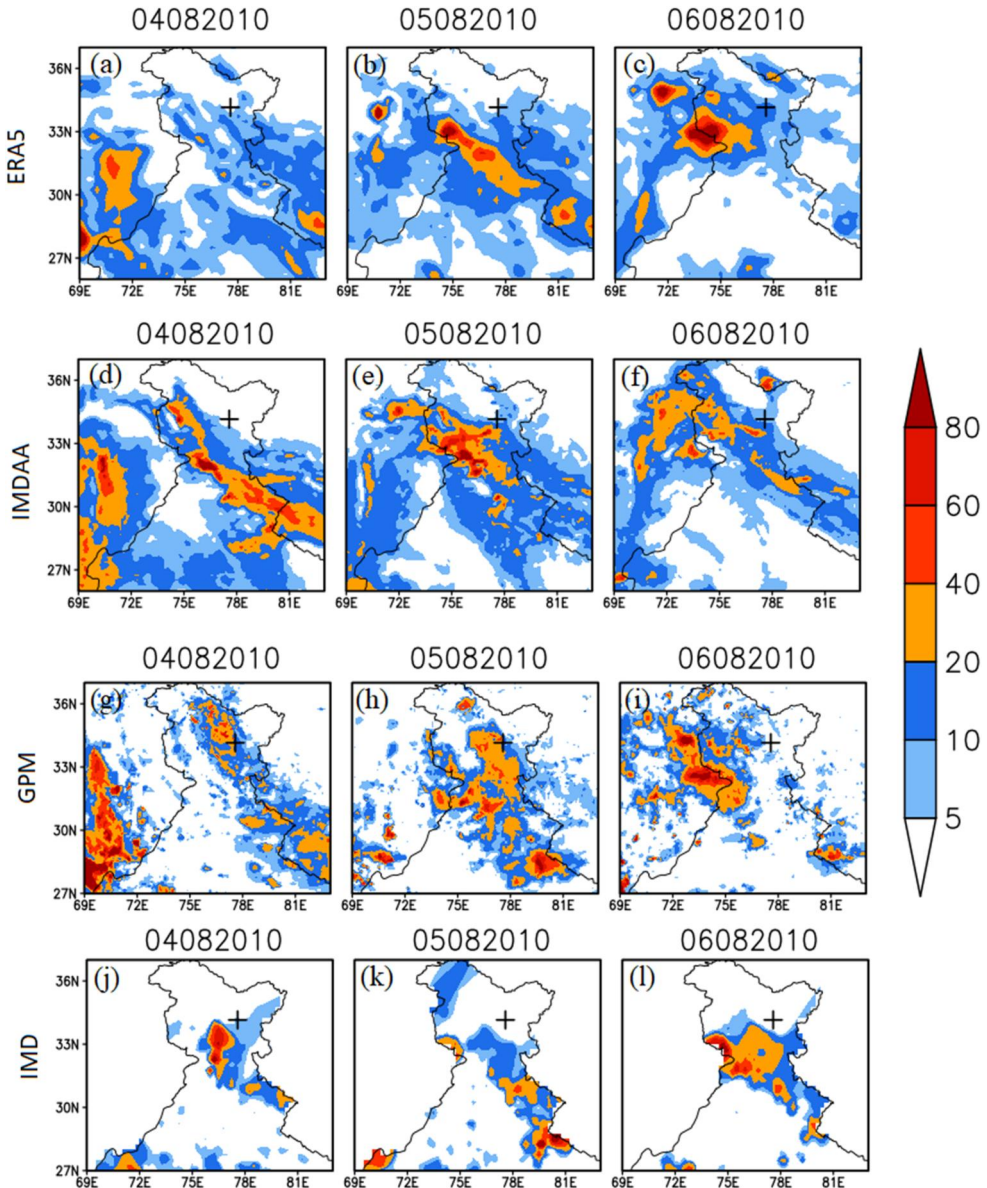


**Figure 7.** (a–l) Same as Figure 5(a–l) but for the cloudburst ‘B’.

The analysis suggests that there is a substantial variation of rainfall for the GPM dataset and diurnal variation in the IMDAA dataset. However, a slight variation is observed in the ERA5 dataset. The ERA5 and IMDAA datasets underestimate rainfall compared to GPM, and there is a discrepancy in the timing of the peak rainfall.

Figure 7(a–l) shows that both datasets ERA5 and IMDAA captured less precipitation for cloudburst ‘B’ than GPM data. ERA5 and IMDAA captured only 10–15 mm of accumulated rainfall on 6August (the day of cloudburst) for cloudburst ‘B’. IMD observations also show less rain over that region due to the non-availability of station data. Figures 8(a–l) and 9(a–l) represent precipitation of cloudburst events ‘C’ and

'D' from ERA5, IMDAA, GPM, and IMD datasets. It is observed from Figure 8(a-l) that all datasets captured low rainfall over that region for event 'C'. IMDAA captures 30% more accumulated precipitation than ERA5 over the selected study region than GPM. However, IMDAA precipitation is significantly less than GPM precipitation as per spatial distribution. For cloudburst 'D', IMDAA captures the spatial distribution of rainfall very well over the region of Uttarkashi compared to ERA5 (Figure 9(a-l)). IMDAA analysis shows a similar trend to the GPM observation. From Figure 6(d), it is observed that the rain rate captured by IMDAA is higher than ERA5 (>5mm/hour). The sudden increase in the rain rate for all three datasets was also noticed at 21UTC on 17 August, which matches the timing of the cloudburst. IMDAA captures a good increment in rainfall during cloudburst time for events 'A' and 'C'; the pattern

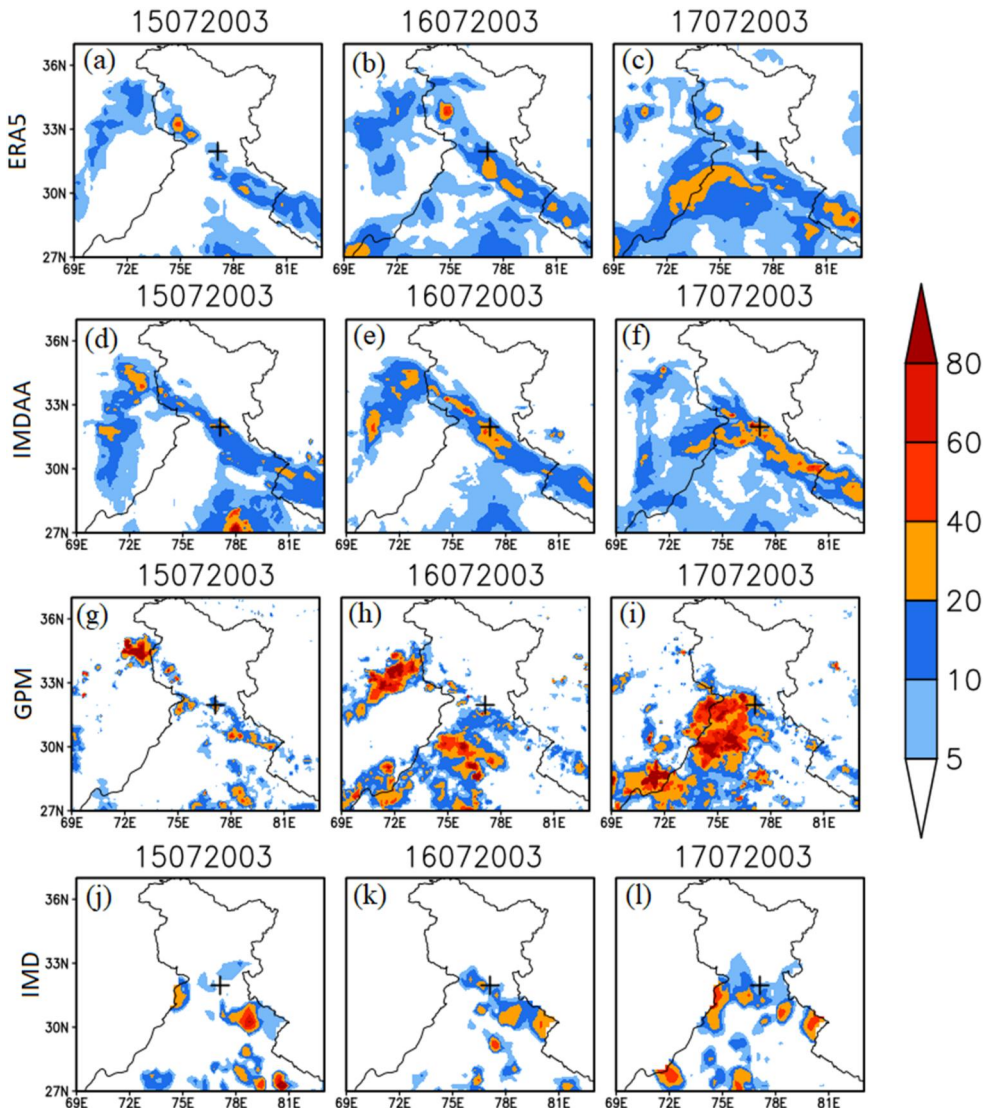
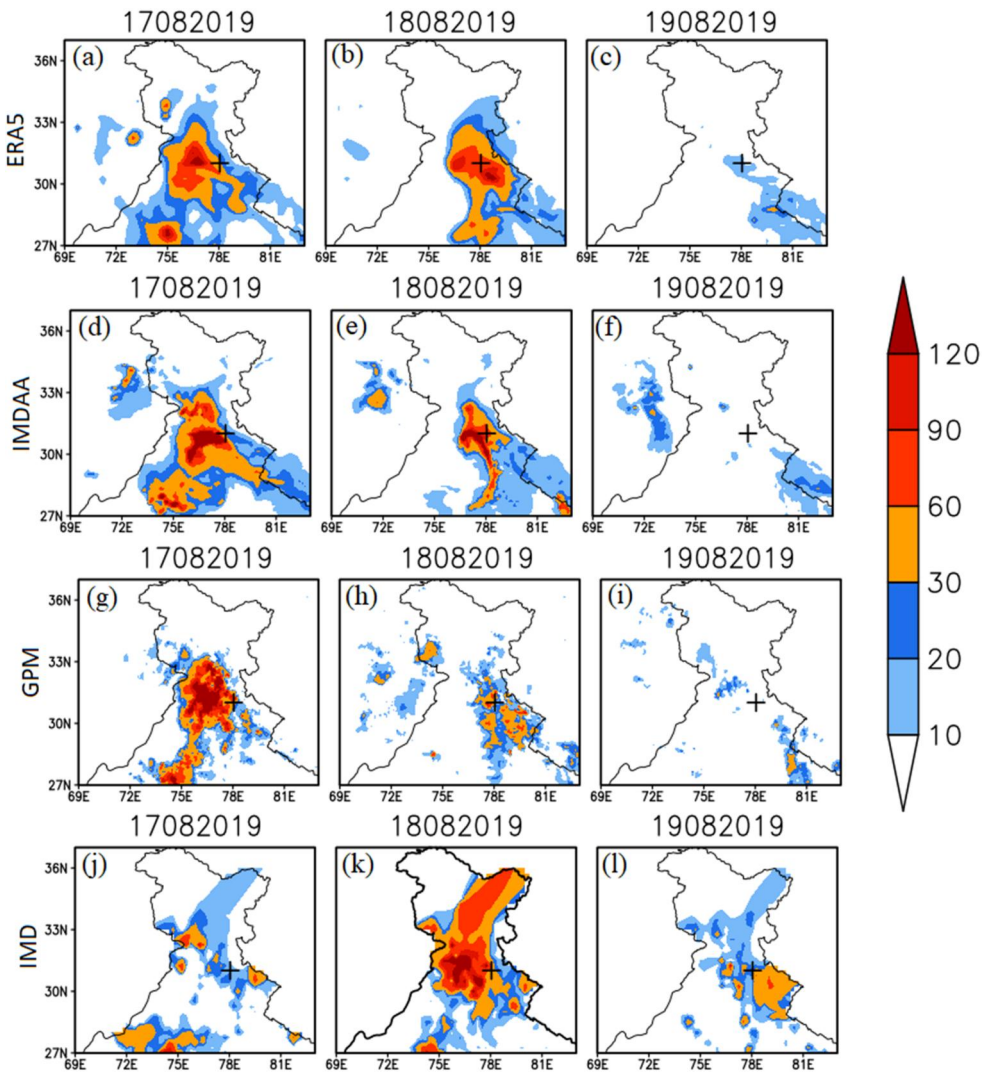


Figure 8. (a-l). Same as Figure 5(a-l) but for the cloudburst 'C'.



**Figure 9.** (a–l). Same as Figure 5(a–l) but for cloudburst ‘D’.

(Figure 6(a,c)) resembles the satellite data. The analysis of cloudburst events shows significant differences in the timing and intensity of precipitation across various datasets. In all instances, the intensity recorded by IMDAA and ERA5 is lower than that of GPM; however, IMDAA is more aligned with observed data compared to ERA5. Additionally, there are noticeable timing differences, with GPM often detecting peaks earlier than the other datasets, likely due to its reliance on satellite retrieval algorithms. IMDAA also exhibits a stronger diurnal variation in precipitation, indicating a better representation of local convection processes. In contrast, ERA5 tends to smooth out short-term fluctuations, limiting its ability to capture localised extreme events accurately.

Table 2 presents the Pearson Correlation Coefficient and Mean Bias Error (MBE) for the ERA5 and IMDAA datasets across four selected cloudburst events over three

days. The correlation coefficients indicate the strength of the relationship between the datasets and observations. IMDAA consistently shows higher correlation values than ERA5 across all events, with mean values of 0.56 and 0.35, respectively. These values suggest that IMDAA captures rainfall patterns more accurately during cloudbursts. The MBE values represent the systematic errors in rainfall estimation, with ERA5 showing an overall mean bias of  $-2.52$  mm and IMDAA at  $-0.74$  mm. Negative MBE values on certain days, especially in ERA5, indicate an underestimation of rainfall, while positive values suggest overestimation. The MBE values indicate that IMDAA exhibits less negative bias than ERA5, highlighting that ERA5 significantly underestimates the rainfall. Overall, IMDAA performs better in terms of both correlation and bias. Reanalysis datasets are expected to underestimate the rainfall compared to observation and observed rainfall due to the inherent challenges in capturing localised intense rainfall events in such products. However, IMDAA captures more precipitation than ERA5, which might be due to its higher spatial resolution and the fact that IMDAA assimilates regional observational data specific to the Indian region(Patel et al. 2023), which enhances its ability to capture localised precipitation events like cloudbursts. However, ERA5, a global reanalysis product, may smooth out such localised extremes due to its coarser resolution and global data assimilation approach.

#### **4.2. Relative humidity**

The high relative humidity (RH) indicates the chance of more precipitation since relative humidity is directly related to rainfall (Pratap et al. 2020). The variation in RH is analysed by plotting the vertical cross-section (pressure levels, time, and RH) in [Figure 10](#). The vertical cross-section of RH is critical in understanding the moisture distribution during cloudburst events. [Figure 10\(a,b\)](#) shows the vertical cross-section of RH of cloudburst event ‘A’ from ERA5 and IMDAA datasets. It is observed that the value of RH is above 95% in both datasets from 12UTC of 15 June to 12UTC of 17 June. ERA5 dataset shows this high RH between 700 and 400 hPa, whereas IMDAA captures it between 700 and 500 hPa. Notably, IMDAA records RH values above 95% even near the surface (1000 hPa) during the most intense precipitation period between 18UTC on 16 June and 00UTC on 17 June, indicating more moisture availability near the ground, likely contributing to the heavy rainfall. [Figure 10\(c,d\)](#) shows the RH for the cloudburst event ‘B’ over the Leh region. In [Figure 10\(c\)](#), the ERA5 dataset indicates the maximum value of RH attained at about 95% on 6 and 7 August 2010 near 500hP, but for a short duration compared to cloudburst ‘A’. IMDAA, in contrast, captures relatively lower RH values, with both datasets indicating a weaker RH pattern than cloudburst ‘A’, suggesting less moisture availability and weaker precipitation potential.

For cloudburst event ‘C’, ERA5 could not capture the high RH value. Although, IMDAA captured a good percentage of RH (20% more than ERA5) around 00UTC on 17 July 2013 from 1000 to 750-hPa for a short duration as compared to cloudburst ‘A’ ([Figure 10\(e,f\)](#)). For cloudburst ‘D’, it is observed that both datasets IMDAA and ERA5 captured maximum RH for a considerable time ([Figure 10\(g,h\)](#)). However, ERA5 has a smaller region than the IMDAA for maximum RH. A sudden downfall

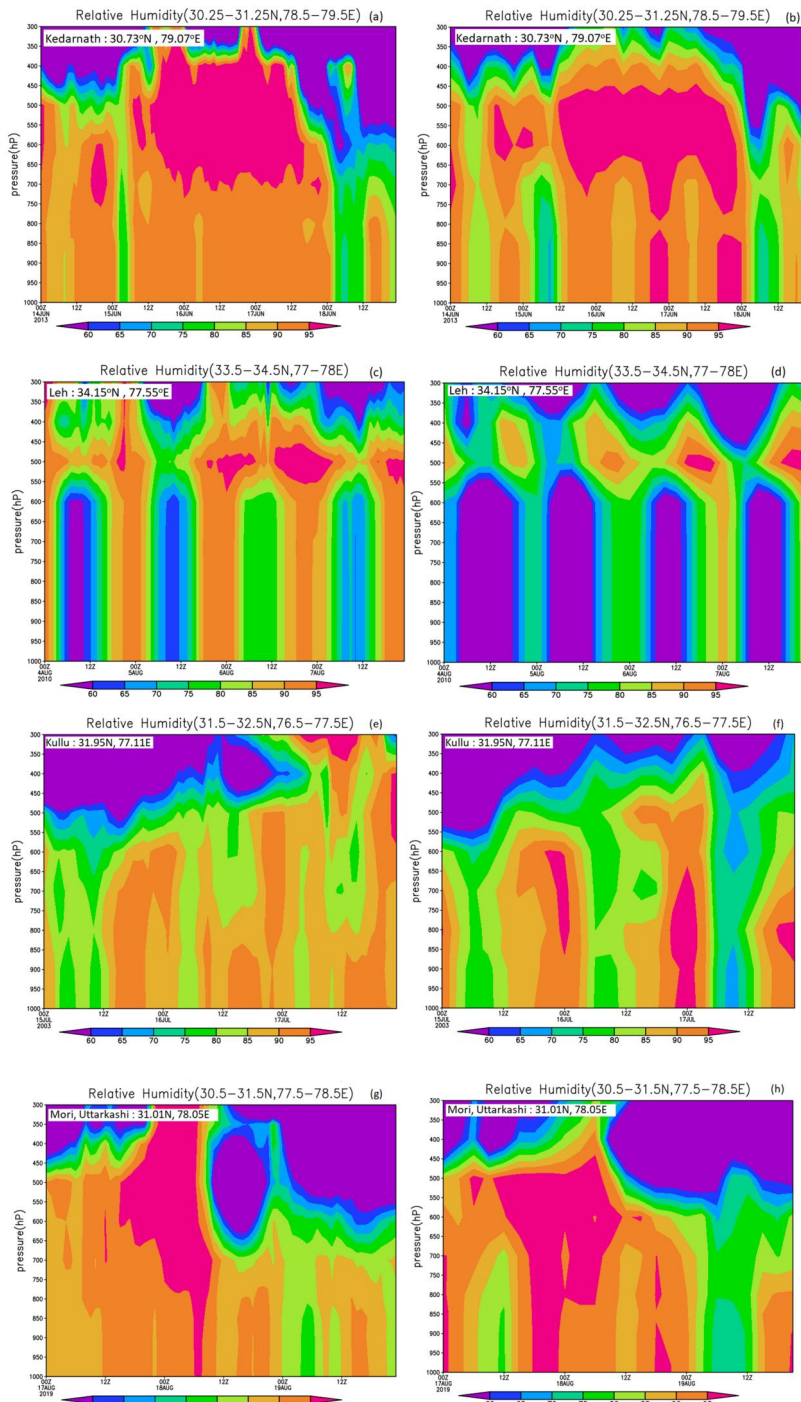


**Figure 10.** Vertical cross-section of relative humidity (rH) in % (a, c, e, g) ERA5 datasets, (b, d, f, h) IMDAA datasets, (a, b) for the cloudburst event 'A', (c, d) for the cloudburst event 'B', (e, f) for the cloudburst event 'C', (g, h) for the cloudburst event 'D'. The region of study is mentioned in the top left of each figure.

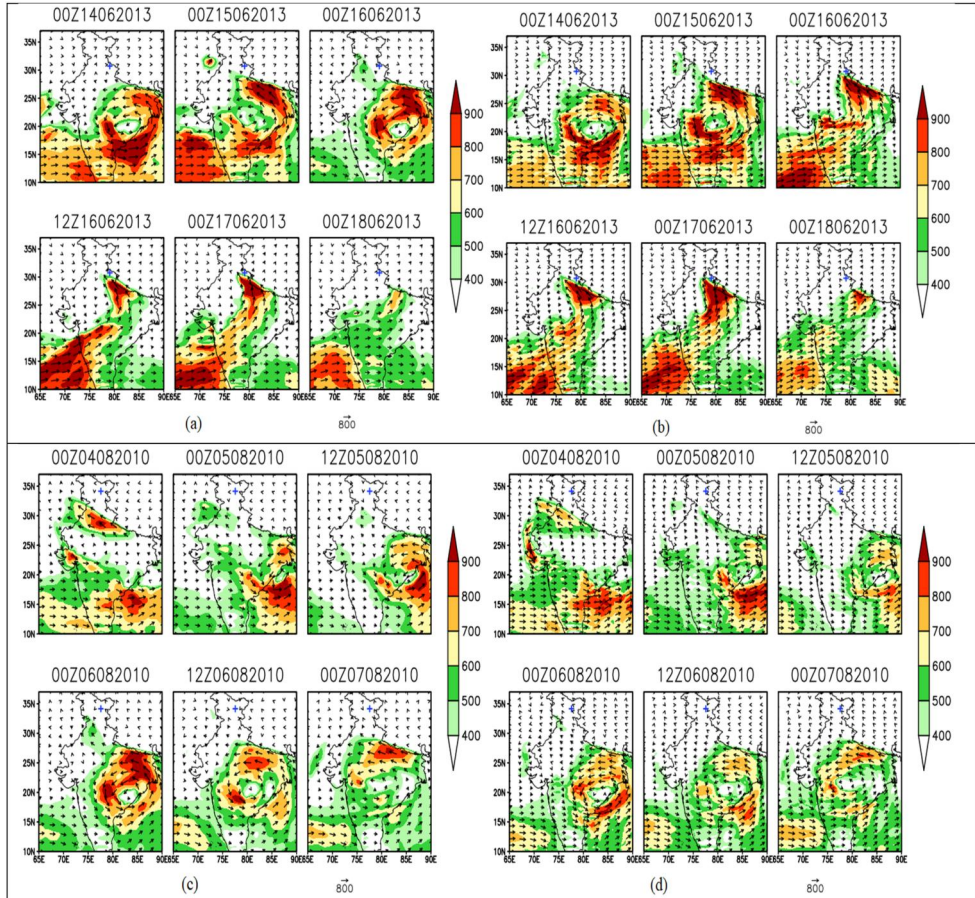


**Figure 11.** Vertical integrated moisture transport (VIMT;  $\text{kg} \cdot \text{m}^{-1} \cdot \text{s}^{-1}$ ; up to 300-hPa) for (a, b). The cloudburst event 'A' (c, d). The event 'B' (e, f). The event 'C', and (g, h). The event 'D'. Left column shows the ERA5 datasets (a, c, e, g) and right column shows the IMDAA datasets (b, d, f, h); time and date are shown on top of each panel.

in RH post cloudburst and a rapid decrease in rain rate is also observed after 00UTC of 18 August (Figure 6(d)).

The differences in RH between the datasets, with IMDAA showing higher RH near the surface and over a broader range in several cases, can be attributed to IMDAA's finer resolution and ability to resolve near-surface moisture better. This leads to more accurate rainfall estimates, especially during the intense phases of the cloudburst events.

#### 4.3. Vertical integrated moisture transport (VIMT)

Vertical Integrated Moisture Transport (VIMT) is a crucial component in understanding the dynamics of cloudburst events, as it represents the transportation of moisture from the ocean to the land surface across various pressure levels. The VIMT

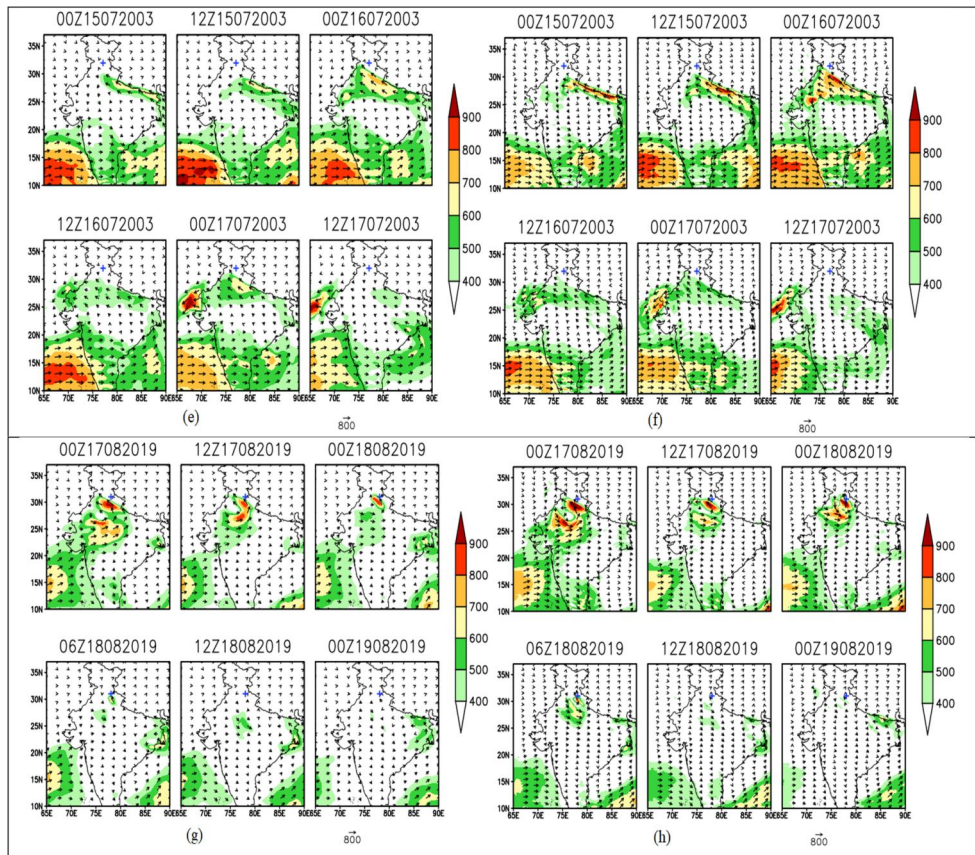


**Figure 11.** Continued.

analyses from surface pressure to 300-hPa levels are shown in Figure 11(a–h) for cloudburst events A, B, C, and D.

For cloudburst event ‘A’, it is evident from Figure 11(a,b) that the primary source of moisture transport is from the Arabian Sea, with the moisture flow initiating over Bihar and East Uttar Pradesh on 14 June 2013. This moisture is then transported northwestward, intensifying until the heavy downpour over Uttarakhand during the night of 16–17 June 2013. Similarly, for cloudburst event ‘D’, moisture transport originates from the Arabian Sea, becoming significant as it traverses East Rajasthan and West Madhya Pradesh, eventually reaching Uttarakhand. The VIMT flux dissipates after the cloudburst event, which coincides with the reduction in rainfall, as seen in Figure 6(d). For cloudburst events ‘B’ and ‘C’, the moisture transport is primarily from the BoB. In cloudburst event ‘B’, vital moisture transport begins at 00 UTC on 6 August 2010, over the region of Bihar. In cloudburst event ‘C’, moisture transport occurs from the western parts of Uttar Pradesh, Delhi, and Haryana towards the northern region, peaking before 00 UTC on 17 July 2013, and weakening afterwards.

The study reveals that the moisture transport mechanisms differ between the events, with events ‘A’, ‘C’ and ‘D’ showing moisture transport predominantly from the Arabian Sea, while event ‘B’ exhibits transport from the Arabian Sea and the BoB.

This transport pattern is consistent across both the ERA5 and IMDAA datasets. However, ERA5 shows higher VIMT magnitude values than IMDAA for cloudburst events. Although there are differences in the magnitude of moisture transport between ERA5 and IMDAA, the overall patterns align well, indicating that both datasets can effectively capture the key atmospheric processes involved in cloudburst formation. These findings highlight the importance of studying VIMT to understand moisture sources and transport pathways during cloudburst events, with both datasets providing valuable insights into these mechanisms. The enhanced VIMT for each event is a critical factor in developing cloudbursts. Still, a moisture threshold is necessary to trigger such extreme rainfall events (Suthinkumar et al. 2023).

#### 4.4. Wind, potential vorticity and geopotential height analysis

Wind magnitude and wind vector field at 500 hPa are analysed in Figure 12, valid at 00UTC for all selected cloudburst events. Figure 13 shows the potential vorticity and geopotential height at 500 hPa level for the four cloudburst events. Cloudburst location is demonstrated by the '+' symbol in each figure. Figure 12(a-f) represent cloudburst event 'A' from ERA5 and IMDAA reanalysis datasets. On 15 June 2013, the wind over Kedarnath originated from the Pakistan Region, with a cyclonic circulation

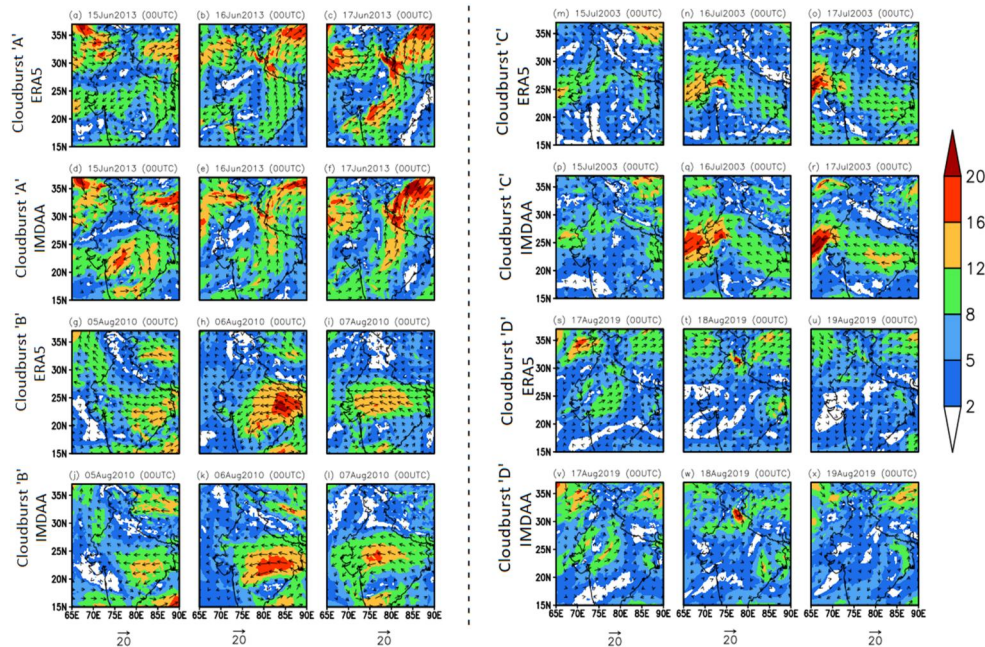


**Figure 12.** Wind magnitude (shaded) & wind direction (vector; m/s) at 500hPa, (a–c) from ERA5 reanalysis dataset and (d–f) from IMDAA datasets for cloudburst event 'A' valid for 00UTC of 15, 16 and 17 June 2013. (g–l) Is same as (a–f) but for cloudburst 'B' valid for 00UTC of 5, 6 & 7 August 2010. (m–r) Is same as (a–f) but for cloudburst 'C' valid for 00UTC of 15, 16 and 17 July 2003. (s–x) Is same as (a–f) but for cloudburst 'D' valid for 00UTC of 17, 18 and 19 August 2019. The '+' symbol indicates location.

over Telangana and its surrounding areas. This westerly wind pattern persists on 16 and 17 June as wind from the Arabian Sea and BoB converges towards the Uttarakhand region, carrying significant moisture (Figure 11(a,b)). As shown in Figure 12(a-f), both wind systems merge over the Kedarnath region, forming extensive cloud cover due to the interaction of moist air and dry air. The topographical orographic effect enhances the formation of clouds, trapping the moisture-laden clouds over the region and contributing to the heavy rainfall on the 16 and 17 June 2013. The potential vorticity at 500 hPa was significantly higher over the Kedarnath region on 16 and 17 June (Figure 13(a-f)) compared to the region's neighbourhood. ERA5 captured potential vorticity very well on 16 June but was unable to capture potential vorticity on 17 June over Kedarnath. In contrast, IMDAA datasets successfully capture high potential vorticity on both days over Kedarnath Region. Furthermore, both datasets indicate a low-pressure area over Uttarakhand, which persists and deepens continuously until the 17 of June, further contributing to the cloud-burst dynamics (Figure 12(a-f)). The analysis highlights the combined role of wind convergence, moisture transport, orography, and potential vorticity in triggering the cloudburst event, emphasising the importance of multi-dimensional atmospheric factors in such extreme weather phenomena.

For cloudburst ‘B’, the 500 hPa wind flow valid 00 UTC on 5 and 6 August 2010 is analysed in Figure 12(g–l). The analysis reveals a robust wind flow over the Tibetan Plateau, moving southwestward towards the Himalayan region. The Tibetan Plateau’s surface significantly impacts circulation over the Himalayan Region during the monsoon season (Yanai and Li 1994). Therefore, heating over the Plateau formed an MCS, and 500 hPa wind flow facilitated the movement of the MCSs towards the Leh region. Simultaneously, moist air from the Arabian Sea and BoB, as part of the

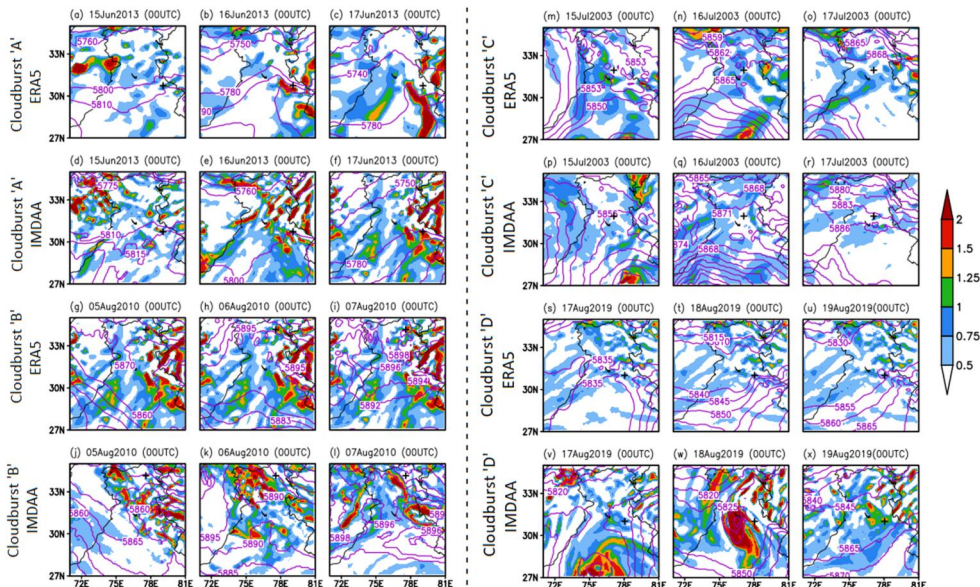


**Figure 13.** Same as Figure 12 but for potential vorticity (shaded; unit-PVU; 1 PVU is  $10^{-6} \text{ K.m}^2.\text{kg}^{-1}.\text{s}^{-1}$ ) at 500 hPa and geopotential height (contour; unit-m) at 500 hPa.

Indian monsoon circulation, was directed towards the Leh region. The interaction of these systems in the Leh region resulted in a heavy downpour. ERA5 and IMDAA datasets captured this wind phenomenon and the associated monsoon troughs during cloudburst 'B'. The spatial distribution of potential vorticity and geopotential height contours are analysed in [Figure 13\(g-l\)](#). This analysis revealed that the potential vorticity intensity over the Leh region is approximately the same in the ERA5 and IMDAA datasets. Both datasets capture the cyclonic activity and atmospheric instability necessary for developing extreme weather events like cloudbursts with similar accuracy.

For cloudburst event 'C', in [Figure 12\(m-r\)](#), the analysis of 500 hPa wind valid for 00UTC on 15, 16 and 17 July 2003 for ERA5 and IMDAA reanalysis shows that on 16 July, warm winds at 500 hPa from the Pakistan region and moist winds from BoB converged near the plains of Haryana, Delhi and Rajasthan, and promoting cloud formation. Low-level winds support these clouds in moving towards the Himalayan region. Due to the absence of high-speed upper-level winds, the clouds were trapped in the region and ended with a heavy downpour. The wind pattern is quite similar for both datasets, although both datasets failed to capture potential vorticity effectively ([Figure 13\(m-r\)](#)). The potential vorticity signature, which typically indicates regions of strong atmospheric instability (Kumar et al. 2018), is weaker and less distinct in ERA5 and IMDAA during this cloudburst event. This suggests that the finer details are crucial for fully representing the extreme conditions leading to the cloudburst. The geopotential height analysis reveals a more clearly defined low-pressure area near Kullu in the ERA5 dataset, which likely contributed to the cloudburst by enhancing upward motion and moisture convergence. In contrast, the IMDAA dataset does not show this low-pressure system distinctly, potentially impacting the accuracy of the moisture transport and precipitation patterns simulated during the event ([Figure 13\(m-r\)](#)).

For Cloudburst event 'D' ([Figure 12\(s-x\)](#)), it is observed that the warm wind from the Pakistan region and moisture-laden winds from the Arabian Sea converge over North India on 17 August 2019. At the time of cloudburst, 00UTC of 18 August, IMDAA captures high wind speed over the region of Uttarakhand. It is observed in both datasets that the mixing of warm air with cold air results in a sudden condensation around 00UTC on 18 August 2019. Additionally, IMDAA captured a high value of potential vorticity over the region and displayed a well-marked low-pressure area, contributing to the cloudburst event ([Figure 13\(s-x\)](#)). The ERA5 failed to capture the high potential vorticity during this event, potentially missing critical dynamics associated with the cloudburst.

#### **4.5. Outgoing longwave radiation and soil moisture**

[Figure 14](#) shows the outgoing longwave radiation (OLR) for all cloudburst events listed in [Tables 1](#) and [2](#), using ERA5 and IMDAA datasets. A small value of OLR suggests the formation of clouds over the region. Rainfall ( $\geq 2.5 \text{ mm/day}$ ) probability exceeds 0.9 when OLR is less than  $180 \text{ W m}^{-2}$  and is very low ( $< 0.05$ ) when OLR is greater than  $280 \text{ W m}^{-2}$  (Kripalani et al. 1991). As illustrated in [Figure 14](#), low OLR

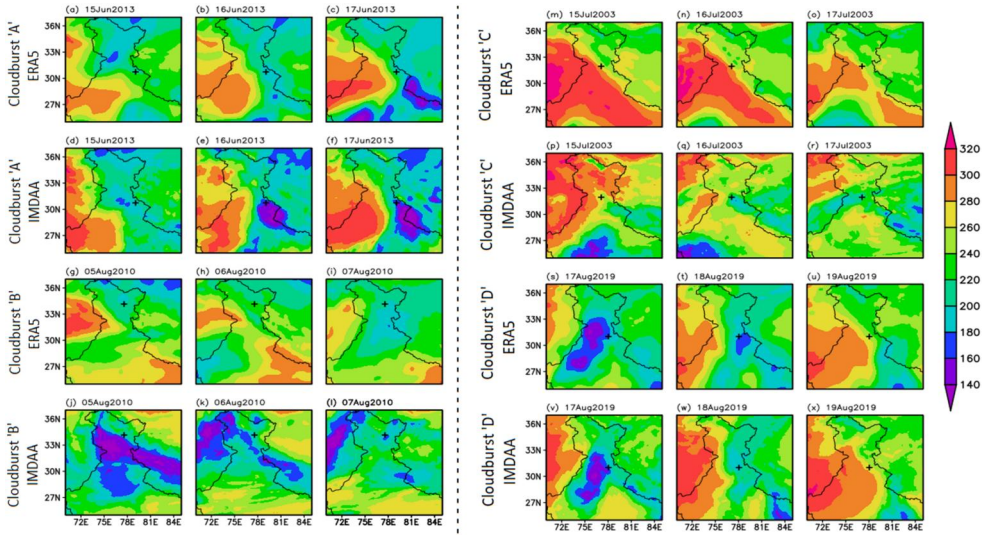


**Figure 14.** Same as Figure 12 but for OLR (shaded;  $\text{W/m}^2$ ).

values are consistently observed across all cloudburst events near their respective regions, confirming the formation of dense cloud systems during these events. For cloudburst event ‘A’ (Figure 14(a–f)), the value of OLR is relatively higher on 15 June 2013 and lower on 16 and 17 June, and there is a sudden increase in OLR value after 18 June onwards, which indicates about the end of the heavy rainfall. The OLR pattern high-low-high values during heavy rain is consistent across all the selected cloudburst events.

However, for cloudburst event ‘C’, the OLR is comparatively higher than in other events. This higher OLR value suggests the possibility of warm clouds forming during this particular cloudburst event. Warm clouds, typically characterised by their inability to reach the freezing level, may still produce significant rainfall, especially under favourable meteorological conditions. Previous studies have demonstrated that warm clouds play a significant role in heavy rainfall events in the tropics, particularly during the monsoon season when moisture availability is abundant but cloud-top heights are relatively lower (Lau and Wu 2003; Zhang and Tao 2013).

Interestingly, the IMDAA dataset consistently captures lower OLR values for all cloudburst events, indicating the formation of clouds and the associated heavy rainfall. On the other hand, while ERA5 also shows a similar temporal pattern, it tends to capture overall higher OLR values ( $\geq 10 \text{ W m}^{-2}$ ) than IMDAA at peak rainfall, this suggests that IMDAA may provide a more accurate depiction of cloud formation and the associated rainfall potential.

In addition to OLR, soil moisture, an essential factor in analysing cloudburst impacts, is shown in Figure 15 for cloudburst events ‘A’ and ‘B’. Soil moisture is expressed as the volumetric water content in the upper soil layer, directly affecting surface runoff, landslide risk, and flash flooding. Both ERA5 and IMDAA datasets tend to capture high soil moisture values during these events, reflecting the heavy rainfall. However, the ERA5 dataset shows slightly higher soil moisture values, as

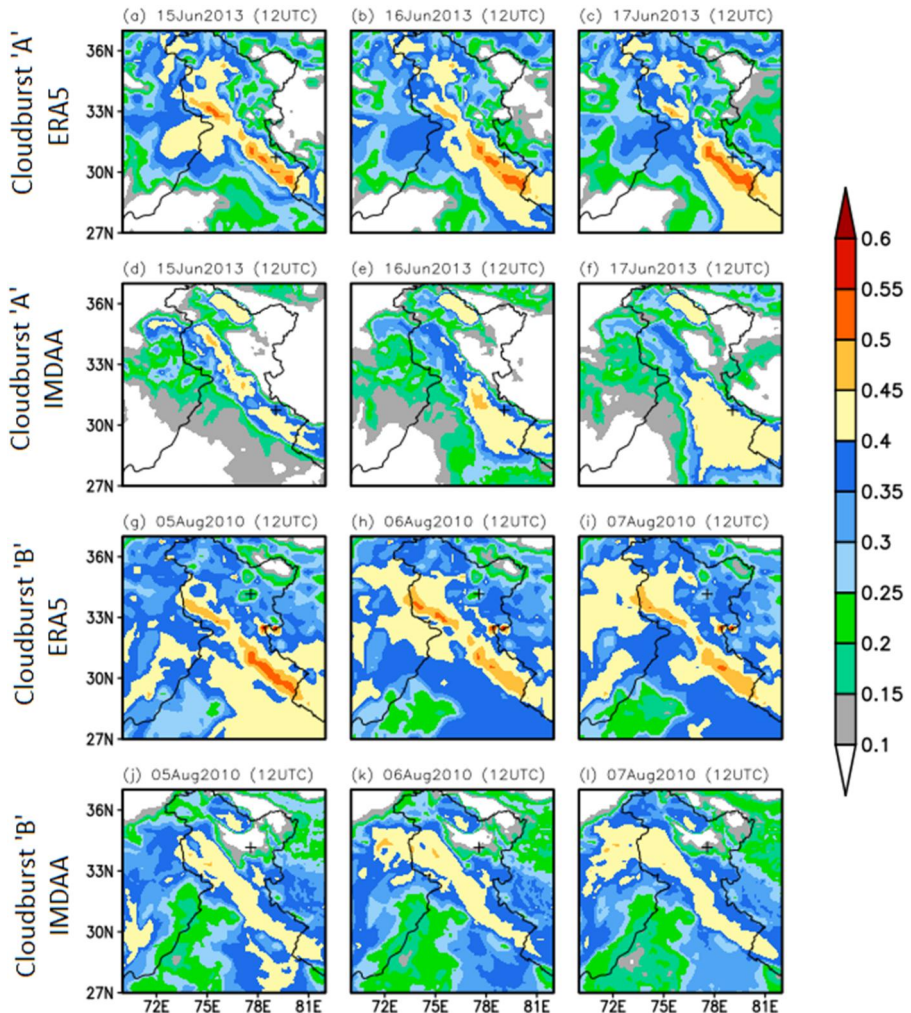


**Figure 15.** Same as Figure 12 but for soil moisture (shaded;  $\text{m}^3/\text{m}^3$ ).

seen in the spatial plots, which may further contribute to the increased risk of landslides and flash floods in the affected regions.

#### 4.6. Vertical velocity/omega

A vertical cross-section of omega (Pa/s) is shown in Figure 16(a–h) for the cloudburst events ‘A’, ‘B’, ‘C’, and ‘D’. The negative value of omega is indicative of the presence of significant upward motion, typically associated with dense cloud formation and precipitation in the region(Patel et al. 2023). In cloudburst event, ‘A’ the heavy rainfall occurs for almost 2–3 days. As depicted in Figure 16(a,b) for cloudburst event ‘A’, omega is highly negative from 12UTC of 15 June to 00UTC of 18 June 2013. Both datasets effectively capture these negative omega values in the mid-troposphere during this period. In contrast, for the cloudburst ‘B’, the ERA5 dataset fails to capture negative omega for cloudburst. Meanwhile, the IMDAA dataset captures a negative

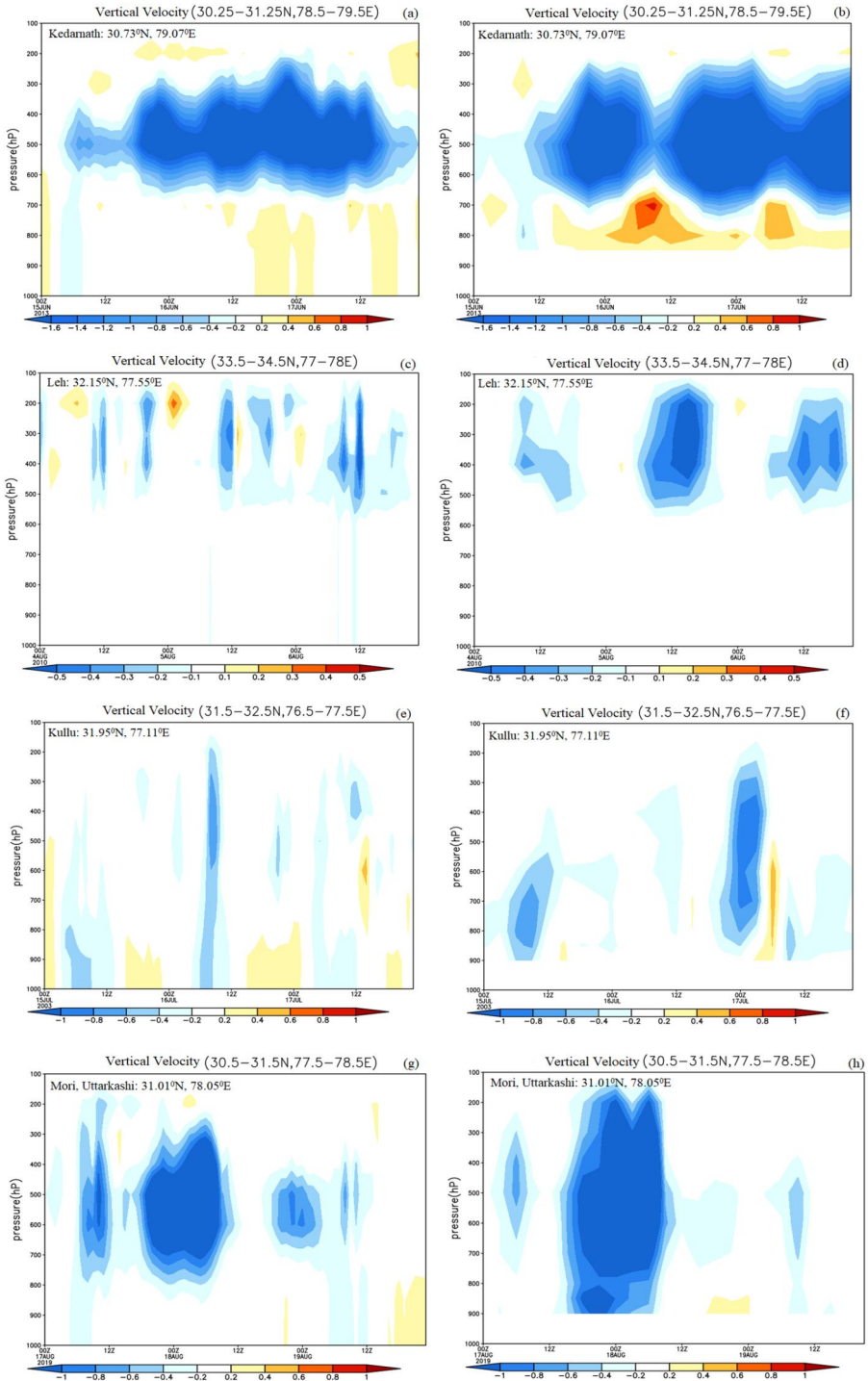


**Figure 16.** Vertical cross-section of omega (Pa/s) for (a, b). The cloudburst event ‘A’ (c, d). The event ‘B’ (e, f). The event ‘C’, and (g, h). The event ‘D’ from ERA5 (a, c, e, g) datasets, and IMDAA (b, d, f, h) datasets. The region of study is mentioned in the top-left panel of each figure, Y-axis pressure level (hPa).

value of omega in the upper troposphere, as seen in [Figure 16\(c,d\)](#). This timing aligns well with the occurrence of the cloudburst over the region.

In the case of cloudburst ‘C’, ERA5 captures the negative value of omega around 06UTC of 16 July 2003, while IMDAA records it around 00UTC of 17 July ([Figure 16\(e,f\)](#)). This difference in timing highlights the temporal resolution differences between the two datasets, which can affect the interpretation of precipitation events. For the cloudburst event ‘D’, both datasets capture negative omega from 18UTC of 17 August to 06UTC of 18 August 2019. However, the IMDAA captures this value in the upper troposphere, whereas the ERA5 dataset fails to capture ([Figure 16\(g,h\)](#)). The high negative omega values during this period correspond to a sudden increase in rainfall, reinforcing the relationship between upward motion and precipitation intensity([Kumar et al. 2018](#)). Overall, the IMDAA dataset consistently captures more pronounced negative omega values for all selected cloudburst events than the ERA5 dataset. This difference suggests that IMDAA is more sensitive to the vertical motion associated with cloud formation, leading to improved insights into the atmospheric processes driving these extreme rainfall events. Such findings underscore the importance of utilising multiple datasets to enhance the understanding of cloudburst dynamics and their associated meteorological factors.

#### **4.7. Stability indices**

Both dynamic and thermodynamic stability indices influence the variation in convection within the atmosphere. The thermodynamic indices, such as the total totals index (TT), severe weather threat index (SWEAT), K index (KI), and lifted index (LI), are computed for all the events selected for the present study. The chances of heavy downpours increase over the region where the stability indices are at critical levels, as shown in [Table 3](#).

[Tables 4–7](#) present the computed values of these indices for all selected cloudburst events. Both the TT and KI indices show elevated values during all cloudburst events, indicating significant instability in the atmosphere. IMDAA consistently captures higher magnitudes for both indices than ERA5, suggesting a more robust signal of atmospheric instability in the IMDAA dataset. These indices, especially TT and KI, provide valuable insights into the likelihood of heavy precipitation associated with each event.

**Table 4.** Thermodynamics indices for cloudburst event ‘A’ averaged over the region (30.25–31.25N, 78.5–79.5E)

Date	TT		SWEAT		KI		LI	
	ERA5	IMDAA	ERA5	IMDAA	ERA5	IMDAA	ERA5	IMDAA
00Z 15 June 2013	46.31	52.94	220.37	251.1	40.22	45.51	-2.57	-7.46
	44.23	51.77	227.00	223.95	36.92	42.75	-1.29	-5.67
	43.53	50.59	249.70	280.23	36.88	48.61	-2.10	-7.14
00Z 16 June 2013	42.40	46.57	266.83	280.4	37.89	40.96	-0.65	-3.48
	41.63	44.43	259.48	265.94	36.82	37.56	-0.09	-2.43
	40.15	45.22	283.96	257.04	35.22	40.95	0.29	-2.26
00Z 17 June 2013	40.98	45.21	273.80	294.24	37.45	44.82	0.07	-2.86
	39.67	45.07	292.36	286.06	37.68	38.36	0.28	-2.24
	40.20	45.44	266.56	287.98	34.34	43.21	-0.38	-3.46

**Table 5.** Thermodynamics indices for cloudburst event 'B' averaged over the region (33.5–34.5N, 77–78E)

Date	TT		SWEAT		KI		LI	
	ERA5	IMDAA	ERA5	IMDAA	ERA5	IMDAA	ERA5	IMDAA
00Z 04 August 2010	39.16	52.18	–	–	34.23	35.89	0.94	-7.19
	06Z	32.83	50.94	–	24.71	32.29	6.4	-5.06
	12Z	31.29	50.06	–	19.77	32.87	6.66	-4.03
00Z 05 August 2010	36.10	51.40	–	–	34.80	48.45	1.95	-8.39
	06Z	32.73	49.42	–	25.35	26.80	5.29	-3.37
	12Z	30.22	52.13	–	19.11	37.58	6.90	-6.04
00Z 06 August 2010	37.46	50.76	–	–	36.68	48.33	1.13	-8.08
	06Z	335.95	53.71	–	31.40	44.08	3.10	-8.66
	12Z	34.21	53.96	–	29.99	42.63	4.24	-8.29

**Table 6.** Thermodynamics indices for cloudburst event 'C' averaged over the region (31.5–32.5N, 76.5–77.5E)

Date	TT		SWEAT		KI		LI		
	ERA5	IMDAA	ERA5	IMDAA	ERA5	IMDAA	ERA5	IMDAA	
00Z 15 July 2003	42.85	46.93	225.56	252.40	37.61	42.48	-1.24	-5.07	
	06Z	41.00	47.40	244.88	243.16	39.02	43.12	0.45	-4.65
	12Z	41.75	47.95	246.50	254.78	42.12	45.21	-1.24	-5.49
00Z 16 July 2003	42.31	48.17	230.35	258.11	40.24	42.27	-1.02	-5.74	
	06Z	42.53	47.78	238.80	242.71	38.23	42.48	-0.27	-4.86
	12Z	42.90	50.27	241.44	257.97	39.13	45.18	-2.22	-6.09
00Z 17 July 2003	43.77	48.87	223.17	264.90	38.35	37.21	-1.84	-6.64	
	06Z	42.66	48.35	232.23	234.10	39.52	42.76	-0.63	-3.86
	12Z	42.76	49.32	247.3	250.70	39.61	43.40	-1.33	-5.74

**Table 7.** Thermodynamics indices for cloudburst event 'D' averaged over the region (30.5–31.5N, 77.5–78.5E)

Date	TT		SWEAT		KI		LI		
	ERA5	IMDAA	ERA5	IMDAA	ERA5	IMDAA	ERA5	IMDAA	
00Z 17 August 2019	42.56	48.60	260.53	301.07	36.89	45.40	-1.22	-6.12	
	06Z	43.98	48.29	281.69	304.40	39.45	44.45	-2.34	-5.80
	12Z	42.94	47.96	286.80	306.3	39.18	42.54	-2.00	-5.20
00Z 18 August 2019	42.06	47.25	302.88	348.72	39.39	42.09	-1.18	-4.35	
	06Z	41.71	46.04	330.98	329.34	38.08	42.18	-1.07	-4.06
	12Z	42.26	45.65	383.80	331.89	37.84	41.29	-0.97	-3.67
00Z 19 August 2019	43.46	47.98	250.17	282.50	37.39	43.33	-1.26	-4.88	
	06Z	45.07	50.14	276.83	268.70	40.56	43.60	-2.11	-5.27
	12Z	46.69	51.70	245.20	260.13	39.60	44.16	-2.78	-6.60

However, the SWEAT index showed moderate values for thunders for cloudburst events 'A' and 'C' while higher values for event 'D'. The SWEAT index is not calculated for event 'B' due to the exclusion of relevant terms in the analysis. Regarding the Lifted Index (LI), ERA5 captured a less negative value, while IMDAA predicted a more negative LI, signifying a more substantial likelihood of thunderstorms in the IMDAA dataset. This further supports the role of IMDAA in identifying more pronounced instability during these extreme weather events.

## 5. Conclusion

The present study investigated the essential characteristics of four cloudburst events in the north-western Himalayan region, utilising reanalysis datasets from ERA5 and IMDAA. A total of fourteen parameters, including rainfall, relative humidity, wind direction, vertical velocity, geopotential height, VIMT, potential vorticity, OLR, and thermodynamic indices, of all events are analysed from both datasets. Overall the findings highlight that IMDAA captures rainfall more effectively than ERA5, with a higher mean Pearson correlation coefficient of 0.56 than ERA5's 0.35. However, both datasets underestimate rainfall amounts. IMDAA shows a smaller bias of  $-0.74\text{ mm}$ , while ERA5 has a more significant underestimation with a mean bias of  $-2.52\text{ mm}$ . This suggests that though both datasets provide valuable insights, IMDAA offers a more accurate depiction of rainfall patterns in cloudburst events.

In addition to rainfall, ERA5 and IMDAA show complementary strengths in capturing other meteorological parameters. ERA5 performs well in capturing relative humidity in the upper troposphere, whereas IMDAA performs better in the lower troposphere. Both datasets represent wind direction accurately, though ERA5 shows a higher magnitude of wind speeds. The VIMT is also an useful indicator in both datasets, showing satisfactory results.

Stability indices, such as the total totals index (TT), K index (KI), and SWEAT index, were also computed for the selected cloudburst events. IMDAA captures these indices near their critical thresholds during thunderstorm events, indicating a higher potential for instability, while ERA5 produces lower values of these indices. This suggests that IMDAA provides a more reliable depiction of atmospheric instability, crucial for studying extreme weather events like cloudbursts. Furthermore, analysis of OLR and vertical velocity highlighted their importance in understanding cloudburst dynamics. IMDAA again outperformed ERA5 in capturing lower OLR values and more robust upward motion, essential for cloud formation and precipitation. The better representation of these parameters in IMDAA makes it a more suitable dataset for analysing cloudburst events.

The results further indicate that IMDAA performs better in studying cloudburst events and general rainfall conditions. Its superior representation of rainfall, atmospheric instability, and key meteorological parameters suggests that IMDAA is the preferred dataset for such studies. However, ERA5 still provides valuable information, particularly in the upper troposphere and wind fields. While this study is based on four cloudburst cases, we acknowledge that a larger sample size would provide more robust conclusions, which will be explored in future work. Also, more modelling studies incorporating multiple events and radar observational data will be necessary to refine our understanding of cloudburst events and improve early warning systems.

## Acknowledgements

The authors acknowledge the data-providing agencies' invaluable contributions to this research. Special thanks to the European Centre for Medium-Range Weather Forecasts (ECMWF) for providing ERA5 reanalysis data, the National Centre for Medium Range Weather Forecasting (NCMRWF) for the IMDAA dataset, and NASA for the GPM satellite data. The authors, N.L. and S.K., are also grateful to the Department of Applied Mathematics, Gautam Buddha University, Greater Noida, UP, India, for their academic and technical support. Additionally,

one of the authors, S.K., extends their appreciation for the infrastructure support received through the Science and Engineering Research Board, (DST-SERB), Government of India's sponsored project (SUR/2022/005506). Finally, the authors acknowledge the anonymous reviewers' suggestions to enhance the quality of the manuscript.

## Disclosure statement

No potential conflict of interest was reported by the author(s).

## Data availability statement

The data used in this research are freely available on the respective institutes' and agencies' websites. The codes used in the analysis are available upon request.

## References

- Ashrit R. 2010. Investigating the Leh "cloudburst". India: National Centre for Medium Range Weather Forecasting, Ministry of Earth Sciences.
- Asthana A, Asthana H. 2014. Geomorphic control of cloud bursts and flash floods in Himalaya with special reference to Kedarnath area of Uttarakhand, India. *Int J Adv Earth Environ Sci.* 2(1):16–24.
- Bannister D, Orr A, Jain SK, Holman IP, Momblanch A, Phillips T, Adeloye AJ, Snapir B, Waine TW, Hosking JS, et al. 2019. Bias correction of high-resolution regional climate model precipitation output gives the best estimates of precipitation in Himalayan catchments. *JGR Atmospheres.* 124(24):14220–14239. doi: [10.1029/2019JD030804](https://doi.org/10.1029/2019JD030804).
- Bhan SC, Paul S, Kharbanda KL. 2004. Cloudburst in Himachal Pradesh. *Mausam.* 55(4):712–713. doi: [10.54302/mausam.v55i4.1441](https://doi.org/10.54302/mausam.v55i4.1441).
- Bhan SC, Devrani AK, Sinha V. 2015. An analysis of monthly rainfall and the meteorological conditions associated with cloudburst over the dry region of Leh (Ladakh), India. *Mausam.* 66(1):107–122. doi: [10.54302/mausam.v66i1.371](https://doi.org/10.54302/mausam.v66i1.371).
- Burton I, Kates RW, White GF. 1993. The environment as hazard. New York: Guilford Press.
- Currier WR, Thorson T, Lundquist JD. 2017. Independent evaluation of frozen precipitation from WRF and PRISM in the Olympic Mountains. *J Hydrometeorol.* 18(10):2681–2703. doi: [10.1175/JHM-D-17-0026.1](https://doi.org/10.1175/JHM-D-17-0026.1).
- Das S, Ashrit R, Moncrieff MW. 2006. Simulation of a Himalayan cloudburst event. *J Earth Syst Sci.* 115(3):299–313. doi: [10.1007/BF02702044](https://doi.org/10.1007/BF02702044).
- Devan H, Panda SK, Mondal U. 2024. Sensitivity analysis of microphysics and cumulus parameterization schemes: numerical simulation of cloudbursts over Uttarakhand using WRF modeling system. *Theor Appl Climatol.* 155(3):1583–1603. doi: [10.1007/s00704-023-04708-6](https://doi.org/10.1007/s00704-023-04708-6).
- Dimri AP, Chevuturi A, Niyogi D, Thayyen RJ, Ray K, Tripathi SN, Pandey AK, Mohanty UC. 2017. Cloudbursts in Indian Himalayas: a review. *Earth-Science Rev.* 168:1–23. doi: [10.1016/j.earscirev.2017.03.006](https://doi.org/10.1016/j.earscirev.2017.03.006).
- Garg S, Tiwari G, Azad S. 2024. Evaluation of the WRF model for a heavy rainfall event over the complex mountainous topography of Mandi, India. *Nat Hazards.* 120(3):2661–2681. doi: [10.1007/s11069-023-06299-x](https://doi.org/10.1007/s11069-023-06299-x).
- George JJ. 1960. Weather forecasting for aeronautics. Vol. 673. New York and London: Academic Press; pp. ix.
- Ghosh S, Barik DK, Renganayaki P, Kang B, Gumber S, Venkatesh S, Saini DS, Akunuri S. 2023. The impact of short-duration precipitation events over the historic Cauvery basin: a study on altered water resource patterns and associated threats. *Sci Rep.* 13(1):1–16. doi: [10.1038/s41598-023-41417-6](https://doi.org/10.1038/s41598-023-41417-6).
- Gumber S, Ghosh S. 2022. Quick predictions of onset times and rain amounts from monsoon showers over urban built environments. *Atmosphere.* 13(3):370. doi: [10.3390/atmos13030370](https://doi.org/10.3390/atmos13030370).

- Gutmann ED, Rasmussen RM, Liu C, Ikeda K, Gochis DJ, Clark MP, Dudhia J, Thompson G. **2012**. A comparison of statistical and dynamical downscaling of winter precipitation over complex terrain. *J Clim.* 25(1):262–281. doi: [10.1175/2011JCLI4109.1](https://doi.org/10.1175/2011JCLI4109.1).
- Hersbach H, Bell B, Berrisford P, Hirahara S, Horányi A, Muñoz-Sabater J, Nicolas J, Peubey C, Radu R, Schepers D, et al. **2020**. The ERA5 global reanalysis. *Quart J Royal Meteorol Soc.* 146(730):1999–2049. doi: [10.1002/qj.3803](https://doi.org/10.1002/qj.3803).
- Hiemstra CA, Liston GE, Pielke RA, Birkenheuer DL, Albers SC. **2006**. Comparing local analysis and prediction system (LAPS) assimilations with independent observations. *Weather Forecast.* 21(6):1024–1040. doi: [10.1175/WAF961.1](https://doi.org/10.1175/WAF961.1).
- Huffman GJ, Bolvin DT, Nelkin EJ. **2015**. Integrated multi-satellite retrievals for GPM (IMERG) technical documentation. NASA/GSFC Code 612 Tech. Doc., 48 pp. Available online at [http://pmm.nasa.gov/sites/default/files/document\\_files/IMERG\\_doc.pdf](http://pmm.nasa.gov/sites/default/files/document_files/IMERG_doc.pdf).
- Kagone S, Velpuri NM, Khand K, Senay GB, van der Valk MR, Goode DJ, Abu Hantash S, Al-Momani TM, Momejiani N, Eggleston JR. **2023**. Satellite precipitation bias estimation and correction using *in situ* observations and climatology isohyets for the MENA region. *J Arid Environ.* 215:105010. doi: [10.1016/j.jaridenv.2023.105010](https://doi.org/10.1016/j.jaridenv.2023.105010).
- Kalnay E, Kanamitsu M, Kistler R, Collins W, Deaven D, Gandin L, Iredell M, Saha S, White G, Woollen J, et al. **1996**. 40-Year reanalysis project. *Bull Am Met Soc.* 77(3):437–470.
- Khanal S, Tiwari S, Lutz AF, Hurk BVD, Immerzeel WW. **2023**. Historical climate trends over high mountain Asia derived from ERA5 reanalysis data. *J Appl Meteorol Climatol.* 62(2): 263–288. doi: [10.1175/JAMC-D-21-0045.1](https://doi.org/10.1175/JAMC-D-21-0045.1).
- Khanduri S, Sajwan KS. **2019**. Flash floods in Himalaya with special reference to Mori tehsil of Uttarakhand, India. *Int J Curr Res Multidiscip.* 4(9):10–18.
- Kripalani RH, Singh SV, Arkin PA. **1991**. Large-scale features of rainfall and outgoing longwave radiation over Indian and adjoining regions. *Contrib Atmos Phys.* 64:159–168.
- Kumar MS, Shekhar MS, Rama Krishna SSVS, Bhutiyani MR, Ganju A. **2012**. Numerical simulation of cloud burst event on August 05, 2010, over Leh using WRF mesoscale model. *Nat Hazards.* 62(3):1261–1271. doi: [10.1007/s11069-012-0145-1](https://doi.org/10.1007/s11069-012-0145-1).
- Kumar A, Gupta AK, Bhambri R, Verma A, Tiwari SK, Asthana AKL. **2018**. Assessment and review of hydrometeorological aspects for cloudburst and flash flood events in the third pole region (Indian Himalaya). *Polar Sci.* 18:5–20. doi: [10.1016/j.polar.2018.08.004](https://doi.org/10.1016/j.polar.2018.08.004).
- Kumar A, Sarthi PP, Kumari A. **2022**. Observed rainfall events and outgoing longwave radiation over contrasting river basins in Bihar, India. *Mausam.* 73(2):273–282. doi: [10.54302/mausam.v73i2.5478](https://doi.org/10.54302/mausam.v73i2.5478).
- Kunz M. **2007**. The skill of convective parameters and indices to predict isolated and severe thunderstorms. *Nat Hazards Earth Syst Sci.* 7(2):327–342. doi: [10.5194/nhess-7-327-2007](https://doi.org/10.5194/nhess-7-327-2007).
- Lau KM, Wu HT. **2003**. Warm rain processes over tropical oceans and climate implications. *Geophys Res Lett.* 30(24):2290. doi: [10.1029/2003GL018567](https://doi.org/10.1029/2003GL018567).
- Litta AJ, Mohanty UC. **2008**. Simulation of a severe thunderstorm event during the field experiment of STORM programme 2006, using WRF-NMM model. *Curr Sci.* 95(2):204–215.
- Maussion F, Scherer D, Finkelnburg R, Richters J, Yang W, Yao T. **2011**. WRF simulation of a precipitation event over the Tibetan Plateau, China – an assessment using remote sensing and ground observations. *Hydrol Earth Syst Sci.* 15(6):1795–1817. doi: [10.5194/hess-15-1795-2011](https://doi.org/10.5194/hess-15-1795-2011).
- Miller RC. **1975**. Notes on analysis and severe-storm forecasting procedures of the Air Force Global Weather Central. Technical report air weather service United States Air Force 200. Air Weather Serv Tech Rep. 200:81–83.
- Mishra A, Srinivasan J. **2013**. Did a cloud burst occur in Kedarnath during 16 and 17 June 2013? *Curr Sci.* 105(10):1351–1352.
- Norris J, Carvalho LMV, Jones C, Cannon F. **2020**. Warming and drying over the central Himalaya caused by an amplification of local mountain circulation. *Npj Clim Atmos Sci.* 3(1):1–11. doi: [10.1038/s41612-019-0105-5](https://doi.org/10.1038/s41612-019-0105-5).
- Pai DS, Sridhar L, Rajeevan M, Sreejith OP, Satbhai NS, Mukhopadhyay B. **2014**. Development of a new high spatial resolution ( $0.25^\circ \times 0.25^\circ$ ) long period (1901–2010) daily gridded rainfall data set over India and its comparison with existing data sets over the region. *Mausam.* 65(1):1–18. doi: [10.54302/mausam.v65i1.851](https://doi.org/10.54302/mausam.v65i1.851).

- Palazzi E, Von Hardenberg J, Provenzale A. 2013. Precipitation in the Hindu-Kushkarakoram-himalaya: observations and future scenarios. *JGR Atmospheres*. 118(1):85–100. doi: [10.1029/2012JD018697](https://doi.org/10.1029/2012JD018697).
- Patel SS, Routray A, Dutta D, Bhatla R, Singh V, George JP. 2023. Studying the evolution of Uttarkashi cloudburst event from reanalysis datasets—a case study. *Dyn Atmos Ocean*. 103: 101387. doi: [10.1016/j.dynatmoce.2023.101387](https://doi.org/10.1016/j.dynatmoce.2023.101387).
- Pratap S, Srivastava PK, Routray A, Islam T, Mall RK. 2020. Appraisal of hydro-meteorological factors during extreme precipitation event: case study of Kedarnath cloudburst, Uttarakhand, India. *Nat Hazards*. 100(2):635–654. doi: [10.1007/s11069-019-03829-4](https://doi.org/10.1007/s11069-019-03829-4).
- Rani IS, Arulalan T, George JP, Rajagopal EN, Renshaw R, Maycock A, Barker DM, Rajeevan M. 2021. IMDAA: high-resolution satellite-era reanalysis for the Indian monsoon region. *J Clim*. 34(12):5109–5133. doi: [10.1175/JCLI-D-20-0412.1](https://doi.org/10.1175/JCLI-D-20-0412.1).
- Ray K, Bhan SC, Bandopadhyay BK. 2015. The catastrophe over Jammu and Kashmir in September 2014: a meteorological observational analysis. *Curr Sci*. 109(3):580–591.
- Sarkar D, Kesarkar A, Bhave J, Goriparthi P, Chandrasekar A. 2024. Synoptic forcing and thermo-dynamical processes during cloudburst event over Sauni Binsar, Uttarakhand, India. *Atmos Res*. 310:107626. doi: [10.1016/j.atmosres.2024.107626](https://doi.org/10.1016/j.atmosres.2024.107626).
- Schultz P. 1989. Relationships of several stability indices to convective weather events in Northeast Colorado. *Wea Forecasting*. 4(1):73–80. doi: [10.1175/1520-0434\(1989\)004<0073:ROSSIT>2.0.CO;2](https://doi.org/10.1175/1520-0434(1989)004<0073:ROSSIT>2.0.CO;2).
- Shah NH, Priamvada A, Shukla BP. 2023. Validation of satellite-based cloudburst alerts: an assessment of location precision over Uttarakhand, India. *J Earth Syst Sci*. 132(4):1–11. doi: [10.1007/s12040-023-02177-z](https://doi.org/10.1007/s12040-023-02177-z).
- Shekhar MS, Pattanayak S, Mohanty UC, Paul S, Sravana Kumar M. 2015. A study on the heavy rainfall event around Kedarnath area (Uttarakhand) on 16 June 2013. *J Earth Syst Sci*. 124(7):1531–1544. doi: [10.1007/s12040-015-0621-6](https://doi.org/10.1007/s12040-015-0621-6).
- Shukla BP, Kishtawal CM, Pal PK. 2017. Satellite-based nowcasting of extreme rainfall events over Western Himalayan region. *IEEE J Sel Top Appl Earth Observ Remote Sens*. 10(5): 1681–1686. doi: [10.1109/JSTARS.2017.2655105](https://doi.org/10.1109/JSTARS.2017.2655105).
- Sikka DR, Ray K, Chakravarthy K, Bhan SC, Tyagi A. 2015. Heavy rainfall in the Kedarnath valley of Uttarakhand during the advancing monsoon phase in June 2013. *Curr Sci*. 109(2):353–361.
- Suthinkumar PS, Varikoden H, Babu CA. 2023. Changes in extreme rainfall events in the recent decades and their linkage with atmospheric moisture transport. *Glob Planet Change*. 221:104047. doi: [10.1016/j.gloplacha.2023.104047](https://doi.org/10.1016/j.gloplacha.2023.104047).
- Thayyen RJ, Dimri AP, Kumar P, Agnihotri G. 2013. Study of cloudburst and flash floods around Leh, India, during August 4–6, 2010. *Nat Hazards*. 65(3):2175–2204. doi: [10.1007/s11069-012-0464-2](https://doi.org/10.1007/s11069-012-0464-2).
- Tyagi B, Krishna VN, Satyanarayana ANV. 2011. Study of thermodynamic indices in forecasting pre-monsoon thunderstorms over Kolkata during STORM pilot phase 2006–2008. *Nat Hazards*. 56(3):681–698. doi: [10.1007/s11069-010-9582-x](https://doi.org/10.1007/s11069-010-9582-x).
- Ullah K, Gao S. 2012. Moisture transport over the Arabian Sea associated with summer rainfall over Pakistan in 1994 and 2002. *Adv Atmos Sci*. 29(3):501–508. doi: [10.1007/s00376-011-0200-y](https://doi.org/10.1007/s00376-011-0200-y).
- Upadhyaya A, Rai AK, Kumar P. 2024. Variability, trends and return periods of extreme rainfall events (EREs) over the north-western Indian Himalayan region (NW-IHR). *Pure Appl Geophys*. 181(8):2631–2650. doi: [10.1007/s00024-024-03542-9](https://doi.org/10.1007/s00024-024-03542-9).
- Wang X, Tolksdorf V, Otto M, Scherer D. 2021. WRF-based dynamical downscaling of ERA5 reanalysis data for high mountain Asia: towards a new version of the high Asia refined analysis. *Intl J Climatol*. 41(1):743–762. doi: [10.1002/joc.6686](https://doi.org/10.1002/joc.6686).
- Yanai M, Li C. 1994. Mechanism of heating and the boundary layer over the Tibetan plateau. *Mon Weather Rev*. 2(112):305–323.
- Zhang F, Tao D. 2013. Effects of vertical wind shear on the predictability of tropical cyclones. *J Atmos Sci*. 70(3):975–983. doi: [10.1175/JAS-D-12-0133.1](https://doi.org/10.1175/JAS-D-12-0133.1).